Nuclear Engineering and Design xxx (2009) xxx–xxx

Contents lists available at ScienceDirect

Nuclear Engineering and Design

journal homepage: www.elsevier.com/locate/nucengdes

Hydride fuel for LWRs—Project overview

E. Greenspan[a,*], M. Fratoni[a], F. Ganda[a], F. Ginex[a], D. Olander[a], N. Todreas[b], P. Diller[b], P. Ferroni[b], J. Malen[b], A. Romano[b], C. Shuffler[b], J. Trant[b], B. Petrovic[c], H. Garkisch[c]

[a] Department of Nuclear Engineering, University of California, Berkeley, CA 94720, United States
[b] Department of Nuclear Science and Engineering, Massachusetts Institute of Technology, Cambridge, MA 02139-4307, United States
[c] Westinghouse Electric Company, 1344 Beulah Rd., Pittsburgh, PA 15235-5083, United States

ARTICLE INFO

Article history:
Received 2 August 2007
Received in revised form 20 June 2008
Accepted 30 November 2008
Available online xxx

ABSTRACT

This special issue of *Nuclear Engineering and Design* consists of a dozen papers that summarize the research accomplished in the DOE NERI Program sponsored project NERI 02-189 entitled "Use of Solid Hydride Fuel for Improved Long-Life LWR Core Designs". The primary objective of this project was to assess the feasibility of improving the performance of pressurised water reactor (PWR) and boiling water reactor (BWR) cores by using solid hydride fuels instead of the commonly used oxide fuel. The primary measure of performance considered is the cost of electricity (COE). Additional performance measures considered are attainable power density, fuel bundle design simplicity, in particular for BWRs, safety, attainable discharge burnup, and plutonium (Pu) transmutation capability.

Collaborating on this project were the University of California at Berkeley Nuclear Engineering Department (UCB), Massachusetts Institute of Technology Nuclear Science and Engineering Department (MIT), and Westinghouse Electric Company Science and Technology Department. Disciplines considered include neutronics, thermal hydraulics, fuel rod vibration and mechanical integrity, and economics.

It was found that hydride fuel can safely operate in PWRs and BWRs having comparable or higher power density relative to typical oxide-fueled LWRs. A number of promising applications of hydride fuel in PWRs and BWRs were identified: (1) Recycling Pu in PWRs more effectively than is possible with oxide fuel by virtue of a number of unique features of hydride fuel-reduced inventory of ^{238}U and increased inventory of hydrogen. As a result, the hydride-fueled core achieves nearly double the average discharge burnup and the fraction of the loaded Pu it fissions in one pass is double that of the MOX fuel. (2) Eliminating dedicated water moderator volumes in BWR cores, thus enabling significant increase of the cooled fuel rod surface area as well as the coolant flow cross-section area in a given fuel bundle volume while reducing the heterogeneity of BWR fuel bundles, thus achieving flatter pin-by-pin power distribution. The net result is an increase in the core power density and a reduction of the COE.

A number of promising oxide-fueled PWR core designs were also found in this study: (1) The optimal oxide-fueled PWR core design features a smaller fuel rod diameter (D) of 6.5 mm and a larger pitch to rod diameter (P/D) ratio of 1.39 than that presently practiced by industry of 9.5 mm and 1.326. This optimal design can provide a 27% increase in the power density and a 19% reduction in the COE provided the PWR can be designed to have the coolant pressure drop across the core increased from the reference 0.20 MPa (29 psi) to 0.414 MPa (60 psi). Under the set of constraints assumed in this work, hydride fuel was found to offer comparable power density and economics as oxide fuel in PWR cores when using fuel assembly designs featuring square lattice and grid spacers. This is because pressure drop constraints prevented achieving sufficiently high power using hydride fuel with a relatively small P/D ratio of around 1.2 or less, where it offers the highest reactivity and a higher heavy metal (HM) loading. (2) Using wire-wrapped oxide fuel rods in hexagonal fuel assemblies, it is possible to design PWR cores to operate at ~50% higher power density than the reference PWR design that uses grid spacers and a square lattice, provided 0.414 MPa coolant pressure drop across the core could be accommodated. Uprating existing PWRs to use such cores could result in up to 40% reduction in the COE. The optimal lattice geometry is $D = 9.34$ mm and $P/D = 1.37$. The most notable advantages of wire-wraps over grid spacers are their significantly lower pressure drop, higher critical heat flux, and improved vibration characteristics.

* Corresponding author.
E-mail addresses: gehud@nuc.berkeley.edu (E. Greenspan), todreas@mit.edu (N. Todreas), petrovb@westinghouse.com (B. Petrovic).

0029-5493/$ – see front matter © 2009 Elsevier B.V. All rights reserved.
doi:10.1016/j.nucengdes.2008.11.023

Please cite this article in press as: Greenspan, E., et al., Hydride fuel for LWRs—Project overview. Nucl. Eng. Des. (2009), doi:10.1016/j.nucengdes.2008.11.023

The achievement of the highest power gains claimed in this study is possible as long as mechanical components like assembly hold-down devices (both in PWRs and in BWRs) and steam dryers (only in BWRs) are appropriately upgraded to accommodate the higher coolant pressure drop and flow velocities required for the high-performance LWR designs. The compatibility of hydride fuel with Zircaloy clad and with PWR and BWR coolants need yet be experimentally demonstrated. Additional recommendations are given for future studies that need to be undertaken before the commercial benefits from use of hydride fuel could be reliably quantified.

© 2009 Elsevier B.V. All rights reserved.

1. Introduction

1.1. Background

This special issue of *Nuclear Engineering and Design* consists of a dozen papers that summarize the research accomplished in the DOE NERI program sponsored project NERI 02-189 entitled "Use of Solid Hydride Fuel for Improved Long-Life LWR Core Designs". The project lasted from September 2002 through January 2006 (Greenspan et al., 2002, 2003). Collaborating on this project were the University of California at Berkeley Nuclear Engineering Department (UCB) – in charge of overall project management (E. Greenspan – PI), neutronics (E. Greenspan), and material compatibility analysis (D. Olander – co-PI); the Massachusetts Institute of Technology Nuclear Science and Engineering Department (MIT) – in charge of thermal hydraulics (T-H), safety, fuel rod vibration and mechanical integrity, and economic analysis (N. Todreas – co PI); and the Westinghouse Electric Company Science and Technology Department (W) – in charge of establishing the data base, defining constraints, and providing general review in light of industrial practice (B. Petrovic – co-PI).

In addition to performance improvements made possible by use of hydride fuel, this study also examined performance improvements in the PWRs using oxide fuel applying the identical set of assumptions as used for the hydride fuel designs. This assures that the comparison between the hydride and oxide fuel designs is on a common basis.

Following this project overview paper is a paper that describes the hydride fuels under consideration, reviews the experience accumulated with hydride fuel, summarizes their physical properties, defines their design constraints, and discusses compatibility issues in the LWR environment (Olander et al., this issue). The following five papers are related to hydride-fueled PWR designs (Ganda et al., this issue-a; Shuffler et al., this issue-a, this issue-b; Diller et al., this issue; Romano et al., this issue). Two design approaches were studied – conventional square lattice fuel assemblies with grid-spacer supports (Shuffler et al., this issue-a) and hexagonal lattice fuel assemblies with wire-wrap supports (Diller et al., this issue). An additional design approach, consisting of inverted geometry PWRs in which the fuel assemblies are made of hexagonal prisms of hydride fuel that are penetrated by vertical cooling channels, is explored in the 12th paper (Malen et al., this issue).

The next three papers are devoted to boiling water reactors (BWRs) (Fratoni et al., this issue; Ferroni et al., this issue; Ganda et al., this issue-b). The scope of the BWR study was more limited than the PWR study. Neutronic and thermal hydraulic analyses were not consistently coupled, vibration analysis was not performed in detail and fuel rod mechanical integrity analysis as well as transient analysis were not performed. Hydrodynamic stability analysis was also not performed; however, the susceptibility of the cores analyzed to instability phenomena was limited by constraining the core average exit quality to the reference core value.

The 11th paper in this series describes a preliminary study that compares the plutonium (Pu) recycling ability of PWRs designed with hydride fuel versus MOX (Ganda and Greenspan, this issue).

1.2. Incentives for hydride fuel

The general objective of this project was to assess the feasibility of improving the performance of PWR and BWR cores by using solid hydride fuels instead of the commonly used oxide fuel. The primary measure of performance considered is the cost of electricity (COE). Other important performance measures are attainable power density, discharge burnup, safety, fuel bundle design simplicity – in particular for BWRs, and Pu transmutation capability.

The primary hydride fuel considered is TRIGA type U–$ZrH_{1.6}$ fuel having 45 wt% U. Properties of this fuel and its compatibility with LWR coolant are briefly discussed in the following section and elaborated upon in a companion paper in this special issue (Olander et al., this issue). The concentration of hydrogen in the hydride fuel is comparable to that of hydrogen in the liquid-phase water of LWR cores. The introduction of part of the hydrogen needed for neutron moderation within the fuel volume permits attainment of an optimal neutron spectrum while using smaller water volume. This feature enables the core to be designed to have optimal moderation, in terms of the attainable discharge burnup, and to have a larger number of fuel rods per unit core volume than a LWR core that uses oxide fuel rods of identical diameter. This feature of hydride fuel could be of particular benefit to BWRs as it enables the elimination of the water rods and, possibly, a reduction of the volume of the water gap between fuel bundles by providing a relatively large hydrogen inventory in the fuel that is fixed and independent of the boiling conditions. Thus, it is expected that hydride-fueled BWR bundles could be designed to be less heterogeneous and to have a higher power density than oxide-fueled bundles. The higher hydrogen concentration per unit core volume is also of benefit for both BWRs and PWRs that are to be designed to transmute Pu and, possibly, minor actinides (MAs).

Hydride-fueled cores have two unique safety-related fuel temperature reactivity feedback mechanisms; one is a prompt and the other is a delayed mechanism. The prompt feedback is due to the reactivity effect of spectrum hardening induced by fuel hydrogen temperature increase that enhances thermal neutron upscattering. It is this negative reactivity feedback that enables operating TRIGA reactors in a pulsed power mode. The other reactivity feedback is due to hydrogen migration out from the fuel into the fuel rod gas plenum. This phenomenon is caused by fuel temperature increase. As the core is designed to be somewhat under-moderated, hydrogen release from the fuel has a negative reactivity feedback effect. This is a delayed effect. Hydrogen exchange between the gas phase and the solid hydride is a reversible process – upon cooling, the hydrogen diffuses back and is absorbed in the fuel. Since this process is very slow compared with the delayed neutron decay time, there will be no difficulty to compensate for the positive reactivity effect of hydrogen concentration increase upon fuel cooling.

Whereas the uranium concentration in U–$ZrH_{1.6}$ fuel is only ~40% of that in uranium dioxide fuel, one of the other hydride materials that is being considered, thorium hydride fuel, (Olander et al., this issue), has a higher HM density than oxide fuel. As a result of this higher HM concentration and larger fuel-to-water volume ratio, cores loaded with thorium–hydride-based fuel may be designed to

Please cite this article in press as: Greenspan, E., et al., Hydride fuel for LWRs—Project overview. Nucl. Eng. Des. (2009), doi:10.1016/j.nucengdes.2008.11.023

have a higher energy generation per core loading and longer core life than the corresponding oxide-fueled cores.

1.3. Hydride fuels considered

The primary hydride fuel considered in this project is uranium–zirconium hydride, similar to that developed by General Atomics (GA) for TRIGA reactors (Simnad, 1980). The U–Zr hydride composition used for the TRIGA fuel has, typically, 1.6 hydrogen atoms per Zr atom, i.e., it is U–$ZrH_{1.6}$. The medium-enriched uranium (MEU) fuel developed by GA for TRIGA reactors contains 45 (w/o) uranium of up to 20 (w/o) ^{235}U (Simnad, 1980). This corresponds to a U/Zr atom ratio of 0.31. The U–Zr hydride fuel considered throughout this project has the same elemental composition. The uranium enrichment is a design variable. This fuel has been in use for more than 40 years in many research reactors around the world in both constant power and pulsed power-operating conditions. It has an impressive record of safety.

The design limits set for the high-power TRIGA core (Iorgulis et al., 1998) are fuel temperatures of 750 °C at steady-state and 1050 °C under transients. Although these temperatures are significantly lower than the maximum permissible operating temperatures of UO_2 fuel, the thermal conductivity of hydride fuel is ~5 times higher than that of oxide fuel. In the high-power TRIGA reactor (Iorgulis et al., 1998) the fuel rod diameter is ~13.8 mm, the fuel-average linear heat generation rate (LHGR) is 37 kW/m, while the peak LHGR is 74 kW/m. The corresponding peak steady-state fuel temperature is 550 °C. For comparison, the average LHGR of an oxide-fueled PWR is 19 kW/m, while the peak value is about 44 kW/m. The TRIGA fuel discharge burnup is ~120 GWD/*t*HM versus <60 GWD/*t*HM for oxide fuel in LWRs. The specific power of the TRIGA fuel is 76 W/g HM versus ~36 W/g HM for the PWR. However, the water temperature in TRIGA cores is more than 200 °C lower than in LWRs so that the LHGR and specific power of hydride fuel in LWRs will be significantly smaller than in the high-power TRIGA. Nevertheless, the analyses performed in this study established that U–$ZrH_{1.6}$ fuel can safely operate in both PWR and BWR cores at as high a LHGR as attainable with oxide fuel.

However, relative to uranium dioxide fuel, U–$ZrH_{1.6}$ fuel has a number of possible drawbacks:

(a) The nominal specific density of U–$ZrH_{1.6}$ at room temperature is 8256 kg/m^3 and the maximum practical U weight % is 45. This makes the atomic density of uranium in U–$ZrH_{1.6}$ only about 40% of that in UO_2 fuel. For Pu and MA recycling, though, the relatively low U loading is an asset rather than a disadvantage – it reduces the inventory of Pu that needs to be loaded per core and increases the fraction of the Pu that is consumed in one cycle (Ganda et al., this issue-c). Moreover, the nominal density of a U–ThH_2 fuel having 25 (w/o) U is 10865 kg/m^3 making the HM density in Th-hydride fuel nearly 12% higher than the U density in UO_2. This may enable increasing the PWR cycle length beyond that attainable using oxide fuel using a similar weight % of fissile material. The relatively low uranium density in hydride fuel will force use of uranium enrichment that is larger than 5% – the current maximum of the nuclear industry. Since there is no technological barrier to handling uranium enriched to higher than 5%, we are assuming that, given sufficient economic incentives, the commercial nuclear industry would successfully petition regulatory agencies to permit use of uranium enriched to more than 5%. An increase in cycle length of thermal reactors and introduction of fast reactors may also require increased enrichment.

(b) Zircaloy (Zy) may not be a compatible clad material for hydride fuel because the hydrogen of the fuel may hydride it. Nevertheless, half-a-dozen approaches have been proposed for protecting the Zy clad using a hydrogen permeation barrier (Olander et al., this issue), including the following: (i) Form a thin oxide layer (~40 μm) over the hydride fuel pellets; it may retain the hydrogen up to 800 °C and will probably avoid fuel-cladding chemical reaction. (ii) Fill the fuel-clad gap with a liquid metal (LM). In addition to providing a hydrogen permeation barrier, the LM will significantly reduce the gap resistance to heat transfer and will enable the design of a wider pellet-clad gap to accommodate the significant irradiation-induced pellet swelling without penalizing the fuel temperature. The feasibility of using LM bonding for LWR UO_2 fuel to improve the heat transfer from fuel to clad and thus reduce the peak fuel temperature, delay onset of fission gas release, avoid pellet-clad interaction, and prevent Zy clad secondary hydriding due to clad failure has recently been found promising by Olander et al. (this issue); it has also been proposed by Wright et al. (1996). The LM is a low melting temperature (~120 °C) alloy of lead, tin, and bismuth at 33 wt% each. There is no experience, though, with LM bonded fuel in the LWR environment.

The feasibility of the proposed hydrogen permeation barriers needs to be carefully studied. The backup approach is to use stainless steel clad.

Experiments done at GA with hydride fuel proved that "high-temperature strength and ductility of the stainless steel or Alloy 800 fuel cladding provides total clad integrity at temperatures as high as 950 °C" (Simnad, 1980). For 12.5%-enriched uranium found in this study to be optimal for use in PWRs, use of SS-304 clad will reduce the attainable discharge burnup by approximately 10 GWD/t relative to that attainable using our selected reference Zy clad. For Pu-bearing fuel, the expected penalty is smaller, due to the higher absorption cross-section of Pu.

(c) If, due to a very severe accident, the hydride fuel temperature significantly exceeds 1050 °C for a prolonged period of time, hydrogen could diffuse out from the fuel into the fission gas plenum. The partial hydrogen pressure with $ZrH_{1.6}$ at 1000 °C is about 20 bar; this is nearly an order of magnitude lower than the fission gas pressure constraint. If the hydrogen gas pressure buildup approaches the gas pressure constraint, it may pose a safety concern.

(d) Hydride fuel may not be compatible with water coolant at PWR and/or BWR-operating conditions. Experiments performed at GA showed that there was no chemical reaction when a very hot (1200 °C) pellet of U–$ZrH_{1.6}$ was dropped into a container of water. Based on the experience with TRIGA fuel, steam–fuel contact and interaction in case of a breach in the clad is not likely to be a safety concern. Nevertheless, due to the higher operating temperatures and pressures of LWRs, there may be a compatibility issue.

Several types of hydride fuels have been examined for this study in addition to U–$ZrH_{1.6}$; they are members of a family of a composite hydride fuel that can be denoted as U–$(Th_nPu_mZr_j)H_x$; the subscripts *n*, *m*, and *j* are the atomic proportions of the metals with respect to uranium, whereas the subscript *x* denotes the atomic ratio of H to the total metals excluding the U. The uranium forms a separate metallic phase because its hydride (UH_3) is unstable at the reactor operating temperatures. The other constituents make a mixed-metal hydride $(Th_nPu_mZr_j)H_x$. The hydrogen density in these fuels is comparable to that in the liquid water of typical PWRs. Even though the experience with and the database for thorium hydride and Pu hydride fuels is small compared with that of zirconium hydride fuel, these fuels are expected to perform comparably, if not superiorly to $ZrH_{1.6}$ fuel. According to Simnad (1986), the developer of the U–$ZrH_{1.6}$ TRIGA fuel, U–ThH_2 is even more stable than U–$ZrH_{1.6}$ fuel and can operate at higher temperatures. Pu also forms a very stable hydride; the equilibrium hydrogen pres-

Please cite this article in press as: Greenspan, E., et al., Hydride fuel for LWRs—Project overview. Nucl. Eng. Des. (2009), doi:10.1016/j.nucengdes.2008.11.023

sure is 1 atm at 870 °C for PuH_2 versus 810 °C for $ZrH_{1.6}$ and 883 °C for ThH_2 (Simnad, 1986).

1.4. Scope of work

The assessment of the COE for hydride versus oxide-fueled cores requires the following core performance characteristics as input: power level, average discharge fuel burnup, HM loading, and uranium enrichment. The power level depends on thermal hydraulic design constraints. The discharge burnup depends on neutronic as well as fuel rod clad integrity design constraints. Safety-related design constraints further limit the acceptable power levels. As a result, a parametric study was performed for PWRs in five disciplines the results from which were fed into the economic analysis – neutronics, steady-state thermal hydraulics, clad integrity, fuel rod vibration, and thermal transient analyses. The study scope for BWRs is limited – it does not include transient and fuel rod performance analysis, fuel rod vibration analysis is not performed in detail and neutronic and thermal hydraulic analyses are not directly coupled. Moreover, the hydrodynamic stability performance of the cores analyzed is not explicitly calculated; rather, the susceptibility of these cores to instability phenomena is limited by constraining the core average exit quality to the reference core value. Consequently, the power gain results for BWRs attributed to hydride fuel should be viewed as upper bound estimates, even though optimization of the hydride design was not performed.

Table 1 summarizes the different systems analyzed along with the range of design variables studied and the design disciplines included in the analysis. Table 2 is a continuation of Table 1; it specifies the design constraints accounted for.

The assessment of the compatibility of U–$ZrH_{1.6}$ fuel with water and with zircaloy clad at typical LWR-operating conditions was to supplement the design optimization studies. The plan was to use TRIGA fuel pellets for these experimental feasibility studies. Unfortunately, we were not able to acquire TRIGA fuel and hence the material compatibility study has been deferred. Instead, we undertook an analytical evaluation of hydrogen redistribution in hydride fuel due to temperature and stress gradients (Olander et al., this issue), and a numerical evaluation of fuel rod performance analysis (Romano et al., this issue).

2. PWR – design approaches and methodology

2.1. Reference reactor

The reference PWR core is defined based on the South Texas Project Electric Generating Station (STPEGS FSAR, revision 12). Selected design and performance parameters of this reactor are summarized in Table 3

2.2. Design approaches

Six different PWR design approaches were examined:

- Uranium oxide fuel using square lattice and grid spacers.
- Uranium hydride fuel using square lattice and grid spacers.
- Uranium hydride fuel using hexagonal lattice and wire wraps.
- Uranium hydride fuel having inverted geometry.
- MOX fuel using square lattice and grid spacers.
- Pu-containing hydride fuel using square lattice and grid spacers.

We will briefly describe the methodology used for our most studied designs – uranium oxide and hydride-fueled PWR cores using a square lattice and grid spacers. Deviations from this methodology introduced in subsequent studies will be defined later. Then in Sections 3–6, results for each of these six different PWR design approaches will be presented.

2.3. Design variables

The primary design variables considered are the fuel rod outer clad diameter, D, and the lattice pitch-to-diameter ratio, P/D. The design space explored is $0.65\,\text{cm} \le D \le 1.25\,\text{cm}$ and $1.074 \le P/D \le 1.54$. Additional design variables considered include the uranium enrichment levels 5, 7.5, and 10% for both oxide and hydride fuels, as well as 12.5, 15, and 20% for hydride fuel, and the coolant pressure drop in the core – 0.20 MPa (29 psi), as of the reference PWR, and 0.414 MPa (60 psi) – assumed attainable with future pumping technology. The number and characteristics of grid spacers are the same as the STPEGS plant.

The uranium dioxide is assumed to be at 95.5% of its nominal density. The zircaloy clad and gap thicknesses are assumed to be functions of the rod outer diameter. For oxide fuel:

For $D \le 7.75$ mm, clad thickness, $t = 0.51$ mm and gap thickness, $\delta = 0.064$ mm

For $D > 7.75$ mm,

$$t\,(\text{mm}) = 0.508 + [D(\text{mm}) - 7.75] \times 0.036$$
$$\delta\,(\text{mm}) = 0.064 + [D(\text{mm}) - 7.75] \times 0.011$$

Hydride-fueled rods have the same clad thickness as oxide rods, whereas the gap thickness is larger due to the larger irradiation-induced swelling characterizing hydride fuel.[2] Such gap thickness, which is burnup dependent, is calculated as the maximum value between 0.076 mm and the value given by the following relation (Garkisch and Petrovic, 2004):

$$\delta(\text{mm}) = 0.5 \times \frac{(D-2t)\times 11.548\times 10^{-3}\times \text{BU}}{1+11.548\times 10^{-3}\times \text{BU}}$$

where D and t are in mm and the BU is given in percentage of U^{235} atoms fissioned out of the total metal atoms (actinides + zirconium) initially present in the fuel.

2.4. Neutronics

The objective of the neutronic analysis is to determine the average discharge burnup of the acceptable geometries. The acceptable geometries are the combination of D and P (or P/D) for which the following reactivity coefficients are negative over the cycle: Doppler, moderator temperature, small void, and large void. In addition to D, P/D, and uranium enrichment, the design variables include the amount of integral fuel burnable absorber (IFBA) or other burnable poisons. The boron concentration in the water is adjusted with burnup to compensate for the remaining excess reactivity.

A special algorithm was developed for predicting in a self-consistent way the discharge burnup and burnup-dependent reactivity coefficients corresponding to a three-batch fuel management based on unit cell calculations. This algorithm (Ganda and Greenspan, 2005c and Ganda, this issue-c) accounts for non-linear k_∞ variation with burnup and for the burnup-dependent soluble boron concentration. It has been benchmarked and found reliable (Ganda and Greenspan, 2005c and Ganda et al., 2005). It is assumed that all three batches are operating at the same average power density and that, at any given time during the cycle, the core average value of parameter $X(t)$ is the arithmetic mean of its value for the

[2] The thermal hydraulic analysis for PWR grids applied the same clad and gap thickness correlations to hydride and oxide fuels. The impact of the larger gap width of hydride fuel was found to be negligible.

Please cite this article in press as: Greenspan, E., et al., Hydride fuel for LWRs—Project overview. Nucl. Eng. Des. (2009), doi:10.1016/j.nucengdes.2008.11.023

Table 1
Summary of design variables and analysis approaches (Y, performed; N, not performed).

System analyzed				Geometry			Thermal hydraulics analysis	Neutronic analysis[a]			Economics
Reactor	Fuel	Rod support	Lattice	D or its range (mm)	P/D or its range	Assembly lattice size, n[b]		Soluble B	BP	U enrichment[c]	
PWR	Oxide	Grid	Square	6.5–12.5	1.07–1.54	$15 \le n \le 20$[d]	Full core	Y	Y	Y	Y
		Wire	Hex	6.5–12.5	1.15–1.42	$15 \le n \le 20$[d]	Full core	Y[e]	Y[e]	Y[e]	Y
	Hydride	Grid	Square	6.5–12.5	1.07–1.54	$15 \le n \le 20$[d]	Full core	Y	Y	Y	Y
		Wire	Hex	6.5–12.5	1.15–1.42	$15 \le n \le 20$[d]	Full core	Y[e]	Y[e]	Y[e]	Y
		None	Inverted hex	N.A.[f]	1.13–1.84	N.A.	Single subchannel	N	N	N	Y (preliminary)
	Pu-hydride	Grid	Square	6.5–12.5	1.05–2	17×17	Assumes as of UO_2	Y	Y	Y[g]	Y (preliminary)
BWR	Oxide	Grid	Square	6–16	1.1–1.6	$4 \le n \le 20$[h]	Full core	N.A.	N	N	
				11.18	1.29	$n = 9$	Single bundle	N.A.	Y	N	
				10.26	1.26	$n = 10$	Single bundle	N.A.	N	N	
	Hydride	Grid	Square	6–16	1.1–1.6	$4 \le n \le 20$[i]	Full core	N.A.	N	N	Y (fuel cost only)
				11.18	1.29	$n = 9$	Single bundle	N.A.	N	N	
				11.18	1.30	$n = 10$, CCCR[j]	Single bundle	N.A.	N	Y[k]	
				10.71	1.30	$n = 10$, CB[j]	Single bundle	N.A.	N	Y[k]	
				10.80	1.30	$n = 10$	Single bundle	N.A.	N	Y[k]	

[a] All the neutronic calculations for PWR are performed using a pin cell model, except for control rods calculations that are done for a fuel assembly. All neutronic calculations for BWR are performed using a single fuel bundle model.
[b] For a square lattice, n is the lattice size ($n \times n$); for a hexagonal lattice, it is the number of rings.
[c] Applicable to uranium-based fuels; for plutonium-based fuel, the amount of plutonium is varied.
[d] n was calculated by an optimization algorithm that varied n between 15 and 20 to obtain the best fit for the assemblies in the reference pressure vessel.
[e] The neutronic characteristics for the wire-wrap designs are inferred from those calculated for the grid-spacer designs.
[f] N.A., not applicable.
[g] Pu concentration is adjusted to give the reference cycle length.
[h] Fuel channel width is fixed.
[i] Fuel channel width both fixed and free to vary.
[j] CCCR, corner cruciform control rod design; CB, control blade design.
[k] 5 and 10% enrichment.

Please cite this article in press as: Greenspan, E., et al., Hydride fuel for LWRs—Project overview. Nucl. Eng. Des. (2009), doi:10.1016/j.nucengdes.2008.11.023

Table 2
Summary of design constraints (Y, applied; N, not applied).

System analyzed				Thermal hydraulics						Neutronics		
Reactor	Fuel	Rod support	Lattice	Steady-state analysis			Transient analysis			Criticality	RC[d]	Cold shutdown reactivity margin
				Basic set[a]	Vibration[b]	Fuel performance[c]	LOCA	LOFA	Over-power			
PWR	Oxide	Grid	Square	Y (no clad T)	Y	Y	Y[e]	Y[e]	Y	Y	Y	Y
		Wire	Hex	Y	Y[f]	Y[g]	Y	N	Y	Y[h]	Y	Y
	Hydride	Grid	Square	Y (no clad T)	Y	Y	Y[e]	Y[e]	Y	Y	Y	Y
		Wire	Hex	Y	Y[f]	Y[g]	Y	N	Y	Y[h]	Y	Y
		None	Inverted hex	Y (no ΔP)	N	N	Y[i]	N	Y	N	N	N
	Pu-hydride	Grid	Square	No T–H analysis was specifically performed	Y	Y	Y					
BWR	Oxide	Grid	Square	Y	Y	N	N	N	N	N	N	N
				Y	N	N				Y	Y	Y
				Y	N	N				Y	N	Y
				Y	Y	N				N	N	N
				Y	N	N				Y	N	Y
	Hydride			Y	N	N				Y	N	Y
				Y	N	N				Y	N	Y
				Y	N	N				Y	Y	Y

[a] MDNBR (or MCPR), pressure drop, fuel average *T* and/or fuel centerline *T*, clad surface *T*, core (bundle) enthalpy rise for full core (single bundle) analysis
[b] Constraints applied to PWRs include: vortex-shedding lock-in, fluid–elastic instability, fretting and sliding wear. Constraint applied to BWRs is rod vibration amplitude.
[c] Fuel performance analysis was independent of rod support method.
[d] Fuel temperature coefficient of reactivity, coolant temperature coefficient of reactivity (excluding BWR); small-coolant void coefficient of reactivity; large-coolant void coefficient of reactivity.
[e] LOCA and LOFA analyses performed for high-power geometries only.
[f] Wear analysis not comprehensive.
[g] Fuel performance limits taken from burnup maps with square lattice powers.
[h] The neutronic characteristics for the wire-wrap designs are inferred from those calculated for the grid-spacer designs.
[i] LOCA analysis performed in a simplified way.

Please cite this article in press as: Greenspan, E., et al., Hydride fuel for LWRs—Project overview. Nucl. Eng. Des. (2009), doi:10.1016/j.nucengdes.2008.11.023

Table 3
Selected design and performance parameters[a] of the reference PWR.

Parameter	Value
Effective core radius (m)	~1.83 (72″)
Active fuel length (m)	4.26 (168″)
Fission gas plenum length (cm)	17.8 (7″)
Clad outer diameter, D (mm)	*9.5*
Square lattice pitch, P (mm)	*12.6*
Pitch-to-diameter ratio	*1.326*
Number fuel rods per core	*50952*
Core enthalpy rise (kJ/kg)	204
Inlet temperature (°C)	294
System pressure (MPa)	15.51 (2250 psi)
Radial peaking factor[b]	1.65
Axial peaking factor	1.55
Power level (MW)	*3800*
Average linear heat rate (W/cm)	*174*
Average power density (W/cm^3)	*99.85*
Average specific power (W/g U)	*38.38*
Average discharge burnup (GWD/*t*)[c]	*50.6*

[a] Parameters in Italics are variables of this study. The other parameters are fixed.
[b] Hottest rod power/average rod power in the core.
[c] Calculated in this project.

three batches, i.e., $[X_1(t)+X_2(t)+X_3(t)]/3$. A more accurate averaging would have been obtained by weighting the batch reactivity by the square of the batch power.[3] However, the batch power strongly depends on the in-core fuel management strategy and the determination of this strategy was beyond the scope of this work.

2.5. Thermal hydraulics

The objective of the thermal hydraulic analysis is to find the maximum power that the core can be designed to operate at for each of the considered geometry combinations of *D* and *P*/*D*, i.e., geometries, while meeting safety-related design constraints. The design constraints considered are a minimum departure from nucleate boiling ratio (MDNBR) of 2.17,[4] average and peak fuel temperature of 1400 °C[5] and 2805 °C[6] for oxide fuel and peak fuel temperatures of 750 °C (steady-state) and 1050 °C (transients) for hydride fuel, and either 0.20 or 0.414 MPa coolant pressure drop across the core corresponding to, respectively, the reference core design or to an upgraded design expected to be practical in the near future (Shuffler et al., this issue-a; Greenspan et al., 2005)

The VIPRE subchannel analysis code was used for the thermal hydraulic analysis. VIPRE predicts the velocity, pressure, temperature, and thermal energy fields as well as MDNBR for interconnected flow channels. MATLAB scripts were developed to drive VIPRE to iteratively determine the maximum power attainable for a given geometry subject to the applicable design limits and to automatically scan the wide range of geometries under consideration (Malen et al., 2004a, b; Shuffler et al., 2006, this issue-a).

2.6. Fuel rod performance analysis

Two independent although related fuel performance analyses were performed: one involved a literature review on past experiments with hydride fuel, a compilation of measured hydride fuel thermo-physical properties, and an analytic evaluation of the expected behavior of hydride fuel in PWR-operating conditions (Olander et al., this issue). The other involved a numerical analysis of the fuel rod mechanical integrity with burnup (Romano et al., this issue). The objective of the latter analysis is to determine the burnup limit the clad can withstand without failure. If this limit is more restrictive (i.e., smaller) than the reactivity limited burnup predicted by the neutronic analysis, it is used in the economic analysis of this geometry.

The fuel rod mechanical integrity analysis considered three clad integrity impairing mechanisms (Romano et al., this issue): (a) Clad corrosion on the water side – the maximum tolerable oxidation thickness is assumed to be 0.1 mm, independent of the fuel rod diameter. (b) Clad strain – the limit is assumed to be 1%, in tension; it includes both elastic and plastic contributions and is due to the external coolant pressure, differential thermal expansion between the fuel and the cladding, fuel swelling due to irradiation, and buildup of fission gases. (c) Clad internal pressure – the maximum acceptable internal gas pressure is assumed 2500 psi. Contributions to the gas pressure buildup accounted for are release of volatile fission products and helium produced by neutron absorption in ^{10}B of the IFBA.

The FALCON and later the TRANSURANUS codes used for the fuel performance analysis simulate the thermal–physical properties of UO_2 fuel pins under steady-state conditions. The following additional assumptions were required to apply these codes to analyze the performance of hydride fuel: (a) the internal pressure constraint was removed due to the very low fraction of fission gas release by hydride fuel (Olander et al., this issue) and (b) thermal expansion and swelling of hydride fuel are ignored since the wide pellet-clad gap together with the liquid–metal bonding assumed in this study allow these effects to be accommodated without straining the clad and without impairing the gap thermal conductance. Based on the above assumptions, the hydride fuel discharge burnup will be limited by the corrosion constraint. For conservatism, the fuel is assumed to operate at the peak LHGR.

2.7. Fuel rod vibration analysis

The objective of this analysis, performed in detail only for PWRs, is to define constraints on the maximum attainable power due to flow-induced vibrations (FIVs) of the fuel rods. Three FIV mechanisms were considered: fluid–elastic instability, vortex shedding lock-in from vortex-induced vibration, and turbulence-induced vibration in cross and axial flows. In addition, two wear mechanisms were considered: sliding wear and fretting wear (Shuffler et al., 2006, this issue-a). The cumulative wear depends on the residence time of fuel in the core, and therefore is a function of both core power and discharge burnup. Five vibration and wear-related constraints were imposed in addition to the steady-state thermal hydraulic design constraints (Shuffler et al., this issue-a)

The outcome of this analysis is the down rating of the core power from the level determined by the steady-state thermal hydraulic analysis subject to the constraints discussed in Section 2.5, as necessary to avoid exceeding any of the vibration constraints. The fuel residence time in the core and, hence, fuel cycle length is adjusted so as to provide the maximum permissible discharge burnup dictated by neutronic and clad integrity analyses.

2.8. Accident and transient analysis

The objective of the accident and transient analyses, performed only for PWRs, was to modify, if necessary, the value of the maximum achievable power derived from the steady-state thermal hydraulic and vibration and wear analyses; the power level of each geometry for which an economic analysis was performed was the smallest of that from the steady-state analysis further truncated by the accident and transient analyses.

[3] The square of the batch power approximates the product of the batch-average product of the flux times the importance function.
[4] The MDNBR limit was derived from a reverse analysis of the STPEGS plant using VIPRE at full power operation using the available Westinghouse W3-L correlation.
[5] Adopted to bound fission gas release to an acceptable value of ~<5%.
[6] To prevent fuel melting.

Please cite this article in press as: Greenspan, E., et al., Hydride fuel for LWRs—Project overview. Nucl. Eng. Des. (2009), doi:10.1016/j.nucengdes.2008.11.023

Due to resource limitations, the safety analysis (Trant, 2004 and Shuffler et al., this issue) was limited to one transient and two accidents:[7] (a) an overpower transient due to a control rod bank withdrawal at full power as defined in the STPEGS FSAR, (b) a large break loss of coolant accident (LOCA), and (c) a complete loss of flow accident (LOFA).

The overpower transient was evaluated with both RELAP and VIPRE codes. RELAP provided the time-dependent power and flow conditions in the core, and the MDNBR was calculated by inputting this information into VIPRE (Shuffler et al., this issue-a).

2.9. Economic analysis

The economic analysis integrates and weights the results obtained in all the analyses described in Sections 2.4–2.8. The objective of the economic analysis is to identify the core geometry (i.e., D and P), which offers the lowest COE when Backfit into an existing PWR. The methodology used for the economic analysis was that laid out by Saccheri et al. (2008); it is based on an OECD/NEA recommended methodology for evaluation of nuclear fuel cycle economics (OECD/NEA, 1994). Although the OECD/NEA cost data and lead times may be outdated, it should be adequate for a relative comparison of different designs.

Two scenarios were considered: (1) A "Minor Backfit" – the reference core fuel assembly and control system layout is maintained. Replacement of the steam generators and modifications to the high-pressure turbine are required to accommodate designs offering higher power than the reference core. Thus, the capital cost investment for Minor Backfit includes the costs to replace the steam generators and upgrade the turbine units if the new geometries offer increased power; it is assumed that the turbine has untapped capacity that can be exploited through a modest capital investment as compared to the costs for complete replacement. Coolant pumps will also require upgrades, but their contribution to the capital investment is relatively small and so will not be considered. (2) A "Major Backfit" – resulting from significant changes to the layout of fuel assemblies and control rods in the core in addition to significant power uprates. This mandates that in addition to steam generator replacement and turbine upgrades, the vessel head and core internals need to be replaced. Coolant pumps will also require upgrades but are not included due to their small relative contribution to the capital cost.

3. PWR – results for square lattice designs

3.1. Neutronics

Fig. 1 gives the attainable burnup for 5%-enriched uranium oxide cores that contain IFBA in the amount of $0.2D/D_{ref}$ mg/cm ^{10}B (core average) where D_{ref} is 0.95 cm, and soluble boron is used to compensate for the rest of the excess reactivity. Geometries exceeding P/D of ~1.4 at large D and all those exceeding P/D ~1.5 have positive coolant temperature coefficient (CTC) of reactivity at BOC.

Fig. 2 gives the discharge burnup attainable from a three-batch core fueled with U–$ZrH_{1.6}$ having 12.5%-enriched uranium – the enrichment level found most economical for hydride fuel. The discharge burnup values displayed in this figure were calculated without accounting for either reactivity constraints or burnable poison and soluble boron. However, a study (Ganda et al., this issue-a) of the six most economic hydride fuel light water lattices concluded that by replacing on the order of 10% of the zirconium hydride by thorium hydride and adding IFBA to the fuel, it is possible to operate the hydride fuel to the same effective burnup as given in Fig. 2 while maintaining all reactivity coefficients negative throughout the cycle. Thus, the burnup values of Fig. 2 represent the discharge burnup expected from hydride fuel in which a relatively small fraction of ZrH1.6 is replaced by ThH2 and IFBA is used as the burnable poison.

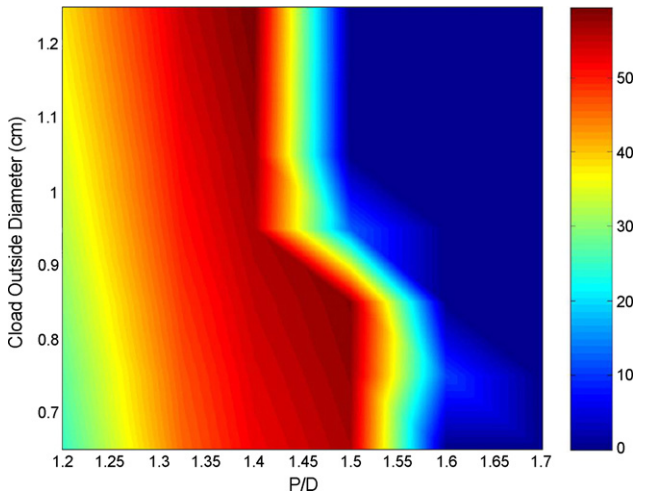

Fig. 1. Attainable burnup in GWD/tHM with 5%-enriched UO_2 accounting for reactivity constraints. Amount of IFBA used is $0.2D/D_{ref}$ mg ^{10}B/cm where D_{ref} is 0.95 cm. Soluble boron compensates for the rest of the excess reactivity.

Alternatively, by loading U–$ZrH_{1.6}$ pellets with erbium as burnable poison, it is possible to decrease the amount of soluble boron required at BOL, with respect to that required with IFBA, and thereby attain negative CTC over the entire geometry range considered. However, the use of erbium involves a few percent penalty in the attainable discharge burnup and is therefore less effective than the replacement of a relatively small amount of zirconium hydride by thorium hydride combined with the use of IFBA. The economic analysis results reported for hydride fuel pertain to U–$ZrH_{1.6}$ fuel in which a fraction of the $ZrH_{1.6}$ is replaced by ThH_2 and to which some IFBA is added. Uranium–thorium–zirconium hydride fuel has been developed and characterized by Yamawaki et al. (1997, 1999), Yamamoto et al. (1998) and Tsuchiya et al. (2000).

Comparison of Figs. 1 and 2 shows that while for oxide fuel the peak burnup is achieved for P/D of ~1.5, for hydride fuel it is obtained for P/D of ~1.2. The smaller optimal P/D for hydride fuel is due to two factors – reduced HM density and inclusion of hydrogen

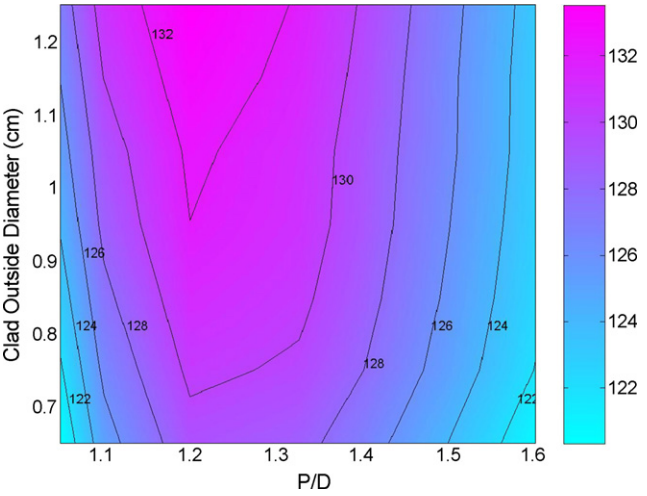

Fig. 2. Attainable burnup in GWD/tHM with 12.5%-enriched U–$ZrH_{1.6}$ without reactivity constraints.

[7] The LOFA accident has not been performed for the hexagonal lattice wire wrapped case.

Please cite this article in press as: Greenspan, E., et al., Hydride fuel for LWRs—Project overview. Nucl. Eng. Des. (2009), doi:10.1016/j.nucengdes.2008.11.023

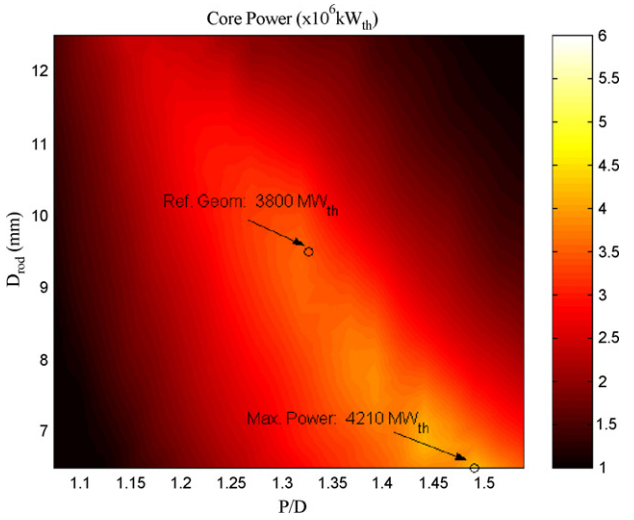

Fig. 3. Maximum achievable steady-state power for UO_2 PWR cores accounting for steady-state and fuel rod vibration and wear constraints. 0.20 MPa core pressure drop constraint.

in the fuel. As a consequence, from the neutronics point of view, more hydride fuel rods of a given diameter can be loaded into a given PWR fuel assembly of a fixed volume than oxide fuel rods.

3.2. Steady-state thermal hydraulics, including vibration and wear

The maximum achievable steady-state power for a UO_2-fueled core as a function of fuel rod diameter and pitch-to-diameter ratio is shown in Figs. 3 and 4, respectively, for 0.20 and 0.414 MPa core pressure drop limits. Steady-state and vibrations and wear constraints are included. It is found that by designing a PWR oxide-fueled core to have smaller fuel rod diameter and larger P/D, it is possible to increase the attainable core power by ~11%, without requiring the pumps to overcome a pressure drop higher than that of the reference core. If, in addition to changing D and P/D, the pressure drop is increased to 0.414 MPa, the attainable power gain is ~31%.

The power achievable with hydride fuel is, in principle, comparable to that achievable with oxide fuel under the same operating

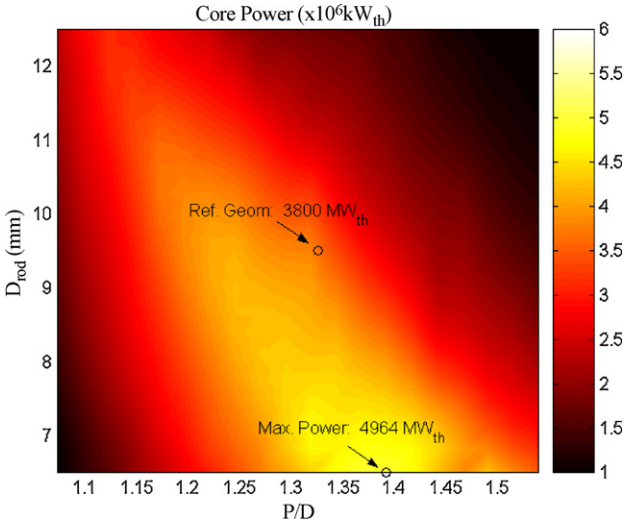

Fig. 4. Maximum achievable steady-state power for UO_2 PWR cores accounting for steady-state and fuel rod vibration and wear constraints. 0.414 MPa core pressure drop constraint.

Table 4
Attainable power levels based on steady-state thermal hydraulic analysis, including vibrations and wear constraints.

	Power (MWh)	Q/Q_{ref}	q'/q'_{ref}	N/N_{ref}	P/D	D (mm)
0.20 MPa						
UO_2 ref. geometry	3800	1	1	1	1.326	9.5
U–$ZrH_{1.6}$ peak power	4210	1.11	0.66	1.68	1.49	6.5
UO_2 peak power	4210	1.11	0.66	1.68	1.49	6.5
0.414 MPa						
U–$ZrH_{1.6}$ peak power	5017	1.32	0.66	2.00	1.37	6.5
UO_2 peak power	4964	1.31	0.67	1.95	1.39	6.5

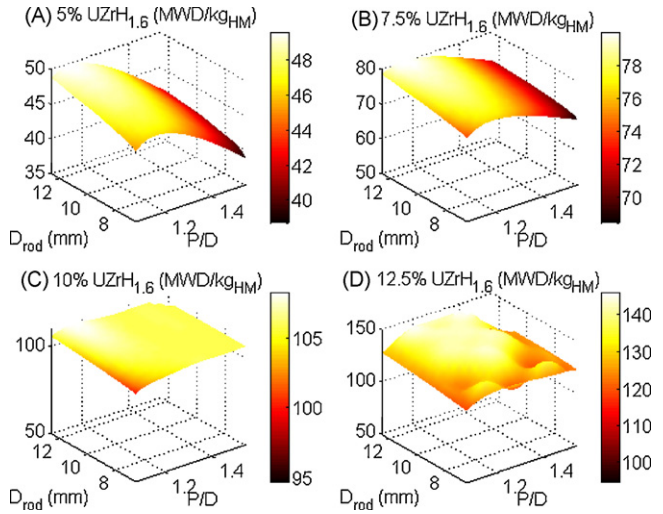

Fig. 5. Maximum achievable burnup for square arrays of hydride fuel with 0.414 MPa pressure drop limit accounting for fuel performance and neutronic constraints.

conditions because both were limited by MDNBR and pressure drop constraints, which apply independent of fuel type. However, as shown in the economic analysis presented in Section 3.6, the minimum COE for a hydride-fueled core is obtained using 12.5%-enriched uranium and for oxide fuel using 5%-enriched uranium. The implication of this is that the optimal hydride fuel residence time is longer than that of oxide fuel, thereby subjecting hydride designs to enhanced vibration induced wear. In order to compensate for the enhanced wear, the power level of the hydride fuel needs to be reduced primarily in the high D and low P design range. Fortunately, this penalty does not affect the peak power core designs. Table 4 compares these peak power designs of hydride and oxide-fueled PWR cores using square lattice with grid-spacers support. Note that the linear heat rates for the peak power geometries are less than that of the reference core. The power gains are therefore obtained by increasing the number of fuel rods in the core, which more than offsets the lower linear heat rate. The design space providing higher linear heat rates than the reference core does not allow an increase in the number of fuel rods with respect to the reference core.

3.3. Clad integrity

For a given geometry, the discharge burnup fed into the economic analysis is the smaller of the fuel performance-limited burnup predicted by TRANSURANUS and the reactivity-limited burnup predicted by neutronic analysis. Figs. 5 and 6 give the attainable fuel performance-limited burnup[8] for, respectively, hydride

[8] The burnup limits imposed due to reactivity constraints are separately specified in Section 3.1.

Please cite this article in press as: Greenspan, E., et al., Hydride fuel for LWRs—Project overview. Nucl. Eng. Des. (2009), doi:10.1016/j.nucengdes.2008.11.023

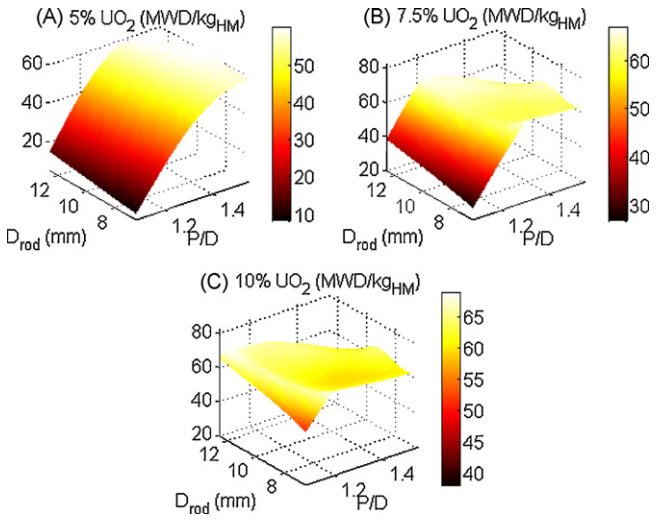

Fig. 6. Maximum achievable burnup for square arrays of oxide fuel with 0.414 MPa coolant pressure drop limit accounting for fuel performance and for neutronic constraints.

and oxide fuel using different uranium enrichments. The results given are for the 0.414 MPa coolant pressure drop limit across the core. Similar results were obtained for a pressure drop limit of 0.20 MPa.

With the exception of very small rod diameters and P/D ratios, the burnup for U–$ZrH_{1.6}$ is limited by the neutronics. UO_2 is limited primarily by neutronics for smaller P/D ratios, and fuel performance for larger P/D ratios, though as the enrichment increases fuel performance takes on a more limiting role.

3.4. Transient analysis

The overpower transient did not reduce the maximum attainable power of either the hydride or oxide-fueled cores relative to that predicted by the steady-state analysis, including vibrations and wear constraints. Likewise, the LOCA did not limit the attainable power for the peak power geometry of either the oxide or hydride-fueled cores.

The LOFA does not penalize the maximum achievable power of the economically advantageous cores for both fuels and for both pressure drops. It does, however, limit the power achievable for the peak power geometry at the higher-pressure drop limit.

Figs. 7 and 8 summarize the results of the accident and transient analyses; they give the maximum attainable power for all core geometries accounting for all the steady-state, vibrations, and overpower transient limits considered in this work for, respectively, 0.20 and 0.414 MPa pressure constrained designs. Due to complexity of the LOFA and LOCA analyses, these transients were only applied to select peak power geometries after application of the other steady-state and transient constraints. Figs. 7 and 8 therefore do not include the LOFA or LOCA constraints. Application of the LOFA constraint to the peak power geometry for both U–$ZrH_{1.6}$ and UO_2 for the 0.414 MPa pressure drop limit reduced the power from 5016 and 4964 MW_{th}, respectively, to 4820 MW_{th}. Application of the LOFA constraint to the peak power geometries at the 0.20 MPa pressure drop limit did not yield any additional power reduction. Applica-

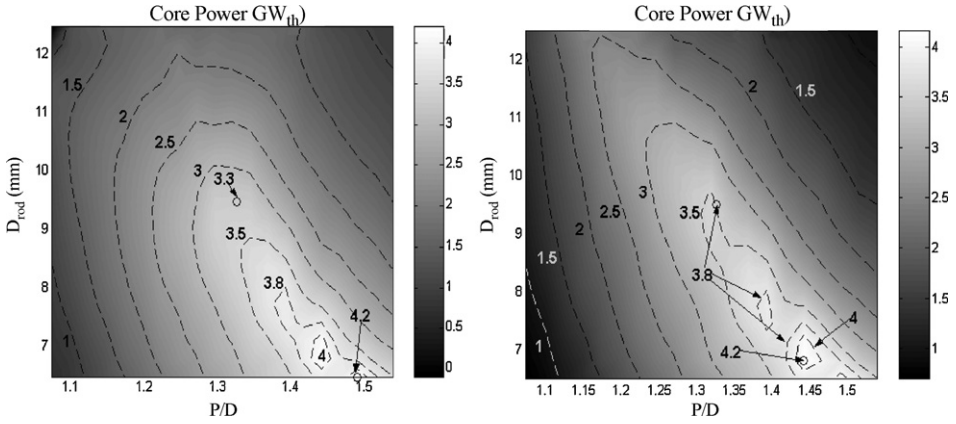

Fig. 7. Maximum achievable power with 0.20 MPa constraint of hydride (left) and oxide (right) cores accounting for all design constraints.

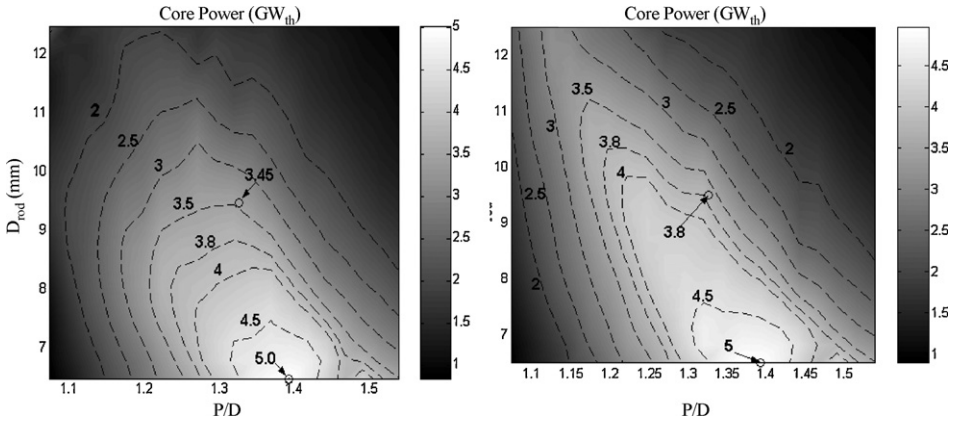

Fig. 8. Maximum achievable power with 0.414 MPa constraint of hydride (left) and oxide (right) cores accounting for all design constraints.

Please cite this article in press as: Greenspan, E., et al., Hydride fuel for LWRs—Project overview. Nucl. Eng. Des. (2009), doi:10.1016/j.nucengdes.2008.11.023

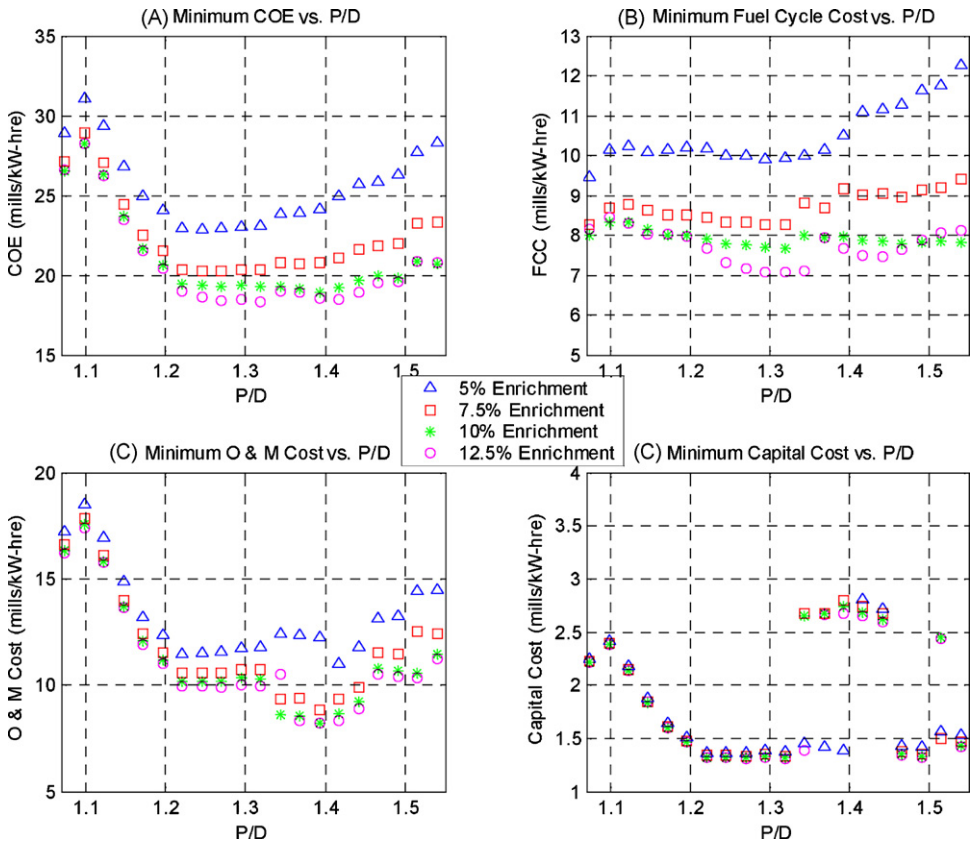

Fig. 9. Minimum COE and its components versus P/D for U–$ZrH_{1.6}$ at 0.414 MPa Major Backfit scenario.

tion of the LOCA constraint to the peak power geometries for both fuels did not result in a further reduction in power.

3.5. Economics

Results of the COE are reported for four cases covering major and Minor Backfit scenarios with 0.414 and 0.20 MPa core pressure drop limits.

3.5.1. Major Backfit scenario with 0.414 MPa core pressure drop limit

Figs. 9 and 10 compare the minimum COE and its components as a function of P/D for hydride and oxide-fueled designs. Not shown in the figures is the fuel rod diameter that gives the minimum COE; its value varies with P/D, enrichment level, and fuel type. For U–$ZrH_{1.6}$, the COE is minimized at the highest enrichment considered. The opposite is true for oxide over the $P/D > 1.25$ range. Also different is the COE trend of variation with P/D. The U–$ZrH_{1.6}$ COE rapidly approaches the most economical geometries as P/D increases and then begins a gradual trend of increased cost due to rising fuel cycle and O&M costs (Fig. 9B and C). The UO_2 COE shows a more gradual descent with P/D. The discontinuity in the capital cost component reflects a transition from geometries that feature the reference or below-reference power level to geometries that offer above-reference power level. The latter geometries require capital cost investment for plant upgrade. In the region where the power is below the reference core power, the capital expenditure (replacement of core internals, vessel head, and remaining value of lost fuel) is fixed and the levelized unit capital cost component depends solely on the power/energy production from the plant.

The minimum lifetime levelized unit COE for the Major Backfit scenario at 0.414 MPa pressure constraint for U–$ZrH_{1.6}$ is found to be 18.34 mills/kWh and is obtained for 12.5%-enriched uranium at $P/D = 1.32$, D[9] = 9 mm. This geometry is very close to the reference core configuration, but over the range of $1.22 < P/D < 1.42$ the COE is within a small fraction of this minimum value. The minimum COE for UO_2 is 18.0 mills/kWh and is obtained for 5%-enriched uranium at $P/D = 1.39$, $D = 6.5$ mm.

Fig. 11, left side, gives the difference in the minimum COE between U–$ZrH_{1.6}$ and UO_2 as a function of P/D ratio and rod diameter. The black contours are the locations of geometries for which the cost difference is zero and the regions are labeled with the fuel giving the minimum COE. The right-hand side of Fig. 11 gives the enrichment level providing the minimum COE for each design point. Hydride fuel offers lower COE in the small P/D, small-to-medium D design range. In this design range, the attainable power is limited primarily by the coolant pressure drop.

It was also found that the specific power and burnup attainable from the hydride fuel far exceed those of the oxide fuel, when both fuels are designed to operate for the same cycle length. The total power and total energy generated per core are, though, comparable. The higher specific power and higher burnup of hydride fuel is due, primarily, to its relatively low HM density. However, to achieve the high burnup, the hydride fuel needs a higher uranium enrichment – 12.5% versus 5% for the oxide fuel.

Whereas for hydride fuel the maximum cycle length and capacity factor are obtained in the low P/D design subspace, where the fuel volume fraction is the highest, for oxide fuel they peak in the high P/D and high D design subspace in which the achievable fuel burnup is relatively high. The power level attainable at

[9] Denoted in some of the figures as D_{rod}.

Please cite this article in press as: Greenspan, E., et al., Hydride fuel for LWRs—Project overview. Nucl. Eng. Des. (2009), doi:10.1016/j.nucengdes.2008.11.023

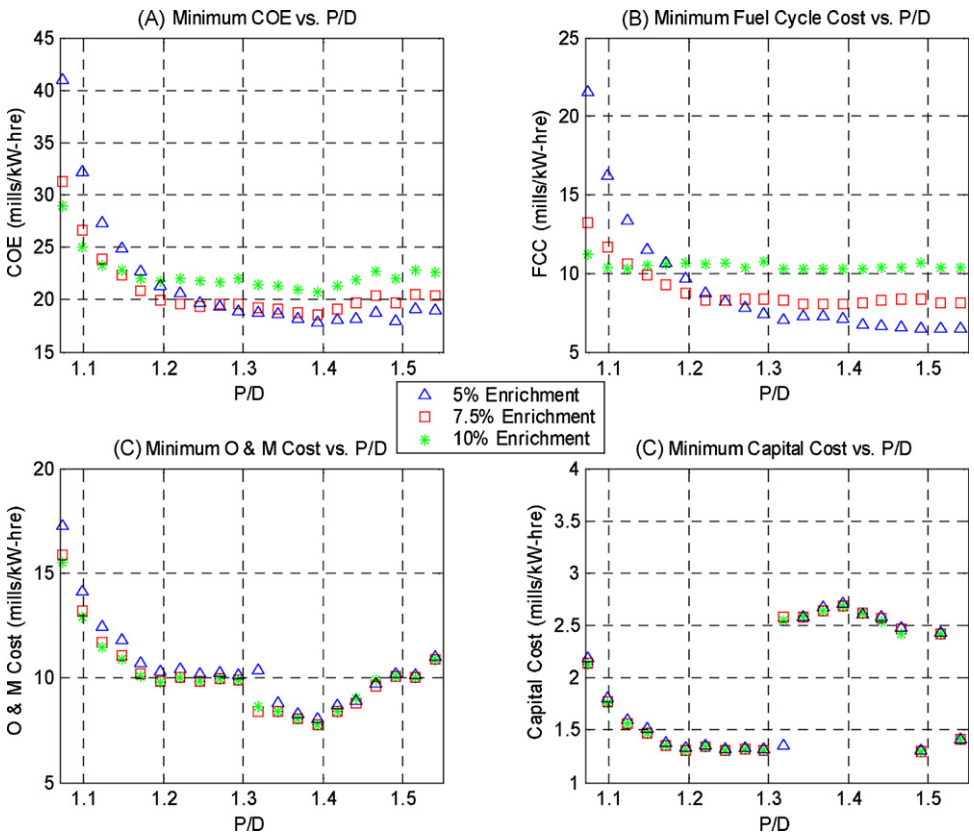

Fig. 10. Minimum COE and its components versus P/D for UO_2 at 0.414 MPa Major Backfit scenario.

the peak cycle length domain for both fuels is, however, relatively low.

3.5.2. Minor Backfit scenario with 0.414 MPa core pressure drop limit

Figs. 12 and 13 compare the minimum COE and its components as a function of P/D for hydride versus oxide fuel for the Minor Backfit scenario at the 0.414 MPa coolant pressure drop. For U–$ZrH_{1.6}$, the minimum COE is 18.9 mills/kWh for 12.5%-enriched fuel, and occurs at P/D ~1.30, D = 9.66 mm. This is slightly higher than the Major Backfit minimum COE of 18.3 mills/kWh. For UO_2, the minimum COE is 18.3 mills/kWh for 5%-enriched fuel, and occurs at P/D ~1.30, D = 9.66 mm. This is slightly higher than the Major Backfit minimum COE of 18.0 mills/kWh.

3.5.3. Major Backfit with 0.20 MPa core pressure drop limit

Figs. 14 and 15 provide a similar comparison for a Major Backfit scenario but for the design limited to 0.20 MPa coolant pressure drop across the core. The minimum COE for U–$ZrH_{1.6}$ is 19.0 mills/kWh for 12.5%-enriched fuel at P/D = 1.37, D = 8.4 mm. The minimum COE for UO_2 is lower at 17.9 mills/kWh for 5%-enriched fuel; it occurs at P/D = 1.47, D = 7.13 mm.

3.5.4. Minor Backfit with 0.20 MPa core pressure drop limit

Finally, Figs. 16 and 17 compare the economics of hydride and oxide fuel designs for a Minor Backfit with a 0.20 MPa pressure drop limit. Like in the higher pressure drop case, the minimum COE for each fuel occurs very close to the reference core geometry. For U–$ZrH_{1.6}$, the minimum COE is 19.3 mills/kWh at P/D ~1.35,

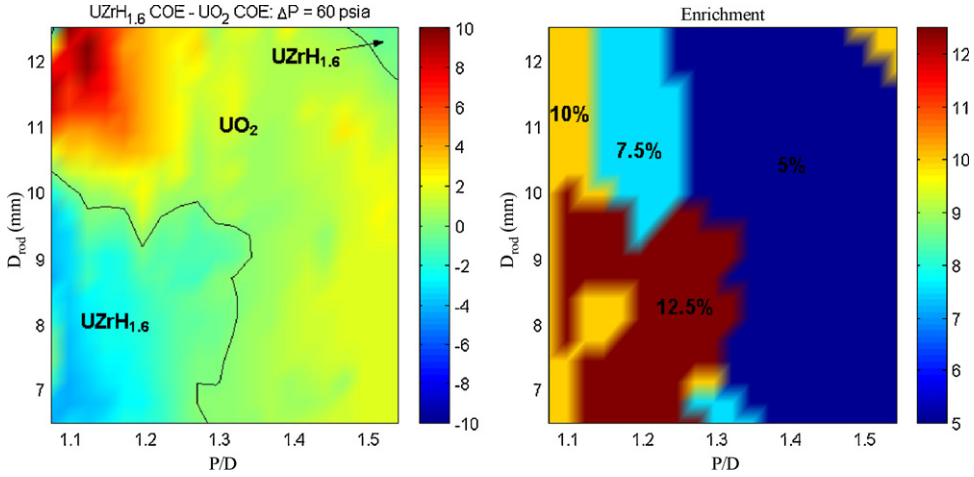

Fig. 11. Lifetime COE difference in (mills/kWh) between hydride and oxide fuel and optimal enrichment of minimum COE fuel at 0.414 MPa and Major Backfit scenario.

Please cite this article in press as: Greenspan, E., et al., Hydride fuel for LWRs—Project overview. Nucl. Eng. Des. (2009), doi:10.1016/j.nucengdes.2008.11.023

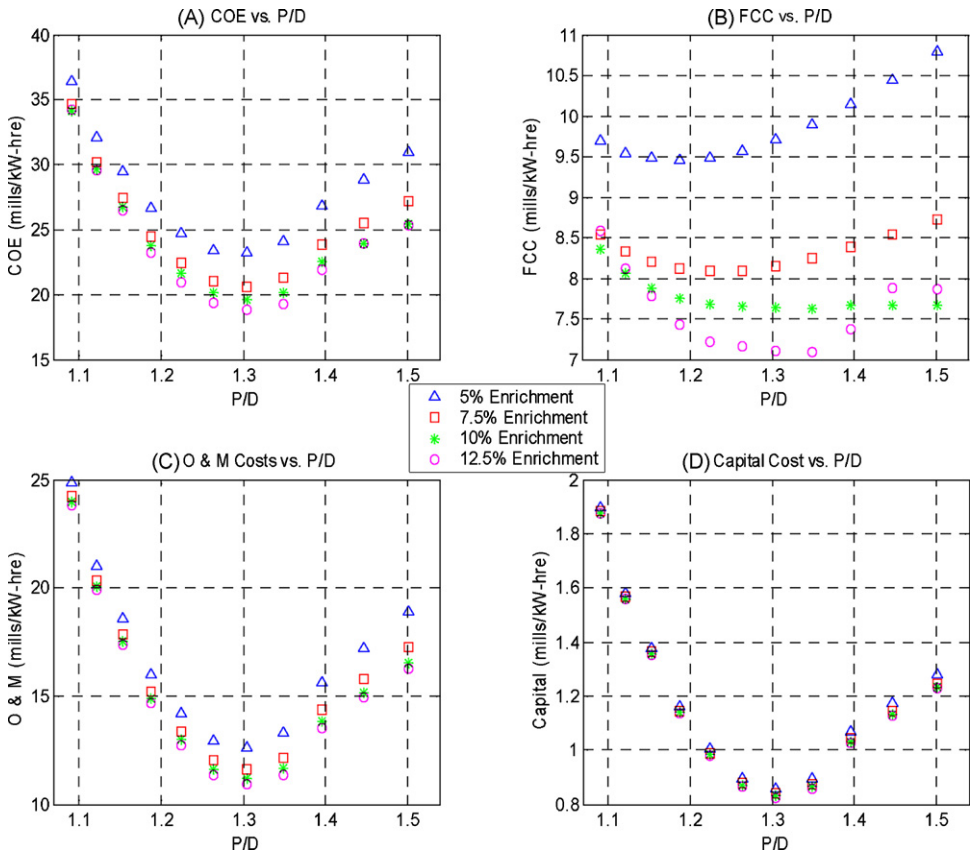

Fig. 12. Minimum COE and its components versus P/D for U–$ZrH_{1.6}$ at 0.414 MPa Minor Backfit scenario.

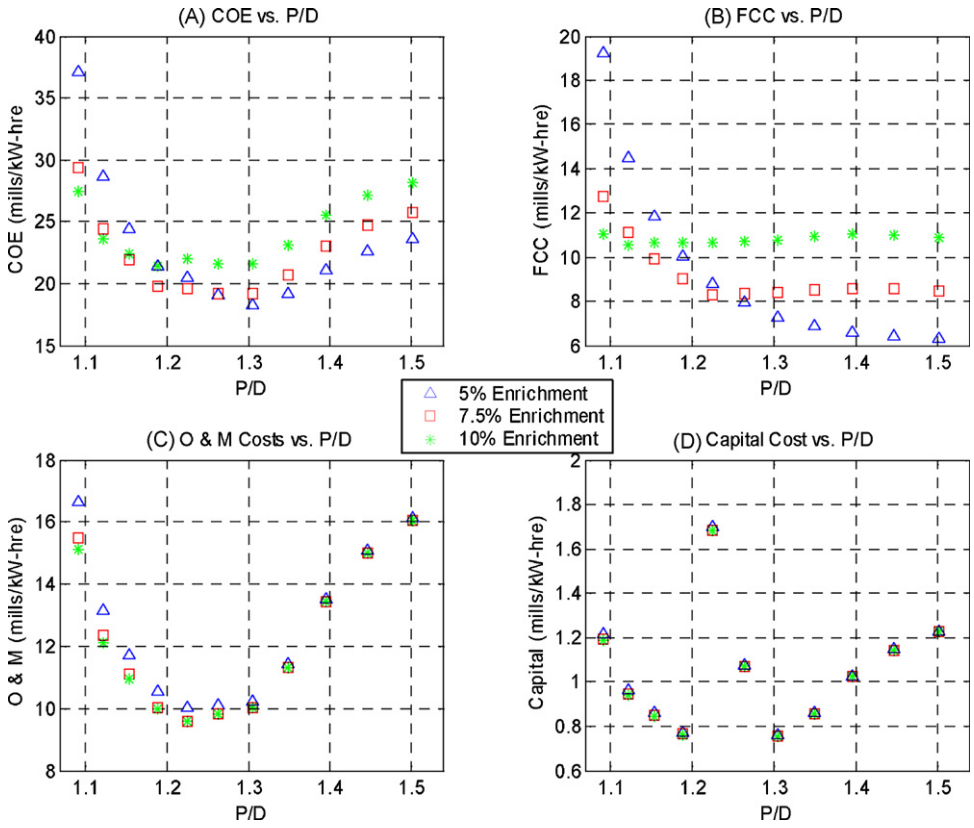

Fig. 13. Minimum COE and its components versus P/D for UO_2 at 0.414 MPa Minor Backfit scenario.

Please cite this article in press as: Greenspan, E., et al., Hydride fuel for LWRs—Project overview. Nucl. Eng. Des. (2009), doi:10.1016/j.nucengdes.2008.11.023

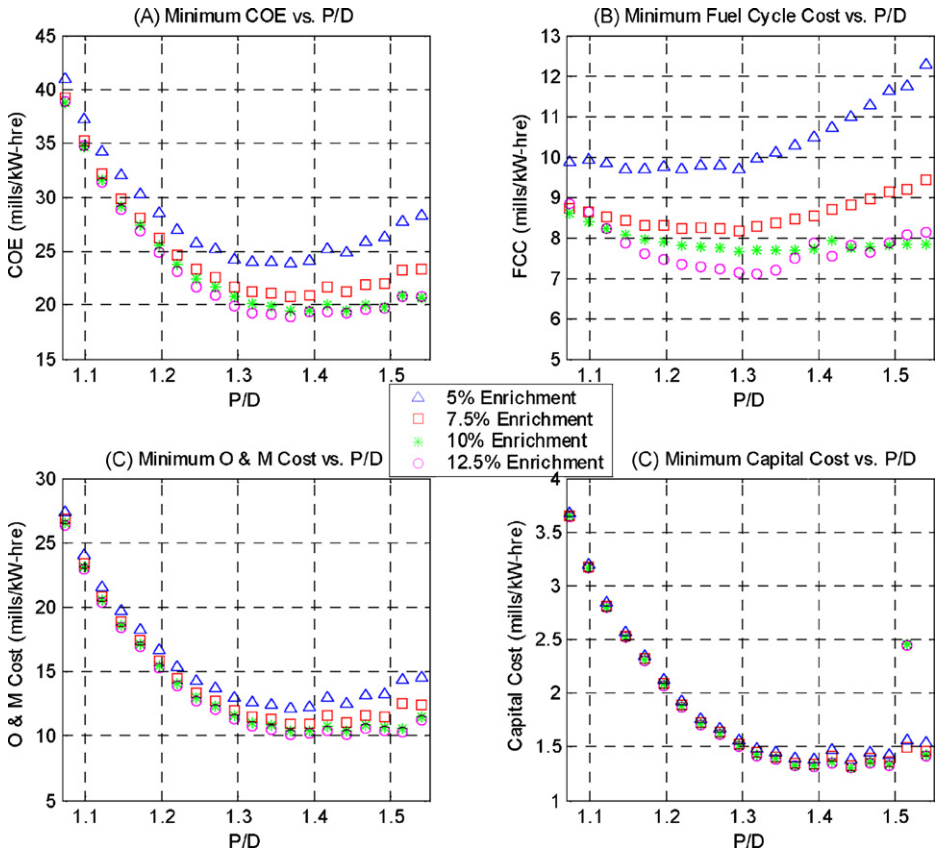

Fig. 14. Minimum COE and its components versus P/D for U–$ZrH_{1.6}$ at 0.20 MPa Major Backfit scenario.

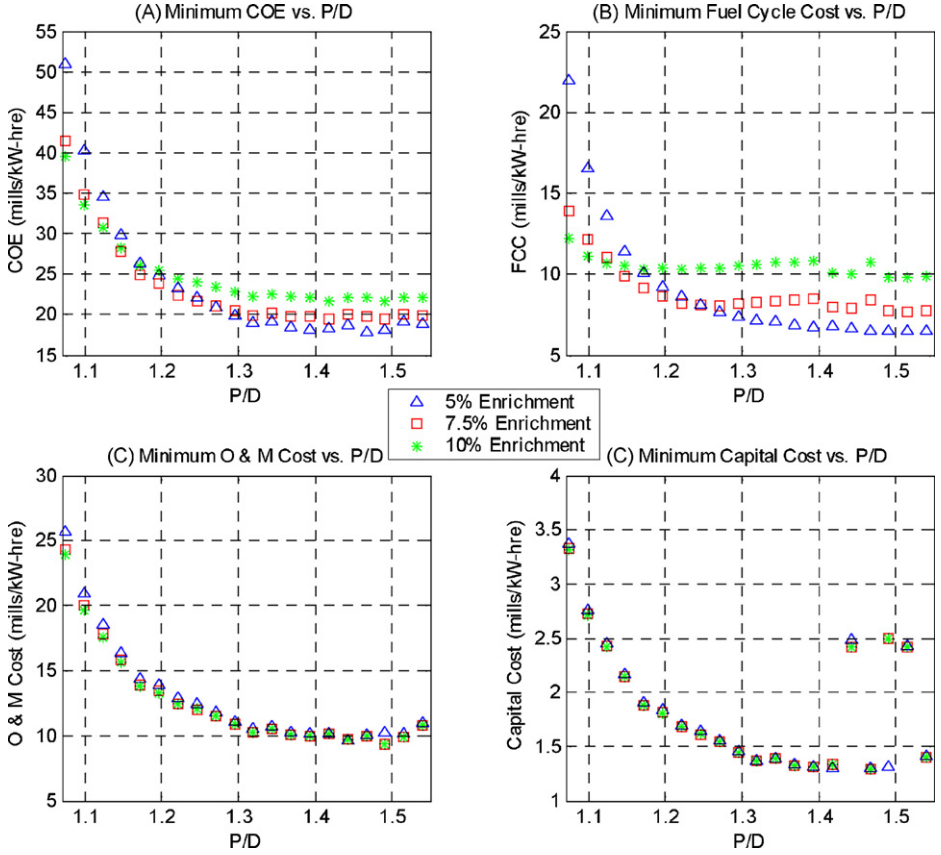

Fig. 15. Minimum COE and its components versus P/D for UO_2 at 0.20 MPa Major Backfit scenario.

Please cite this article in press as: Greenspan, E., et al., Hydride fuel for LWRs—Project overview. Nucl. Eng. Des. (2009), doi:10.1016/j.nucengdes.2008.11.023

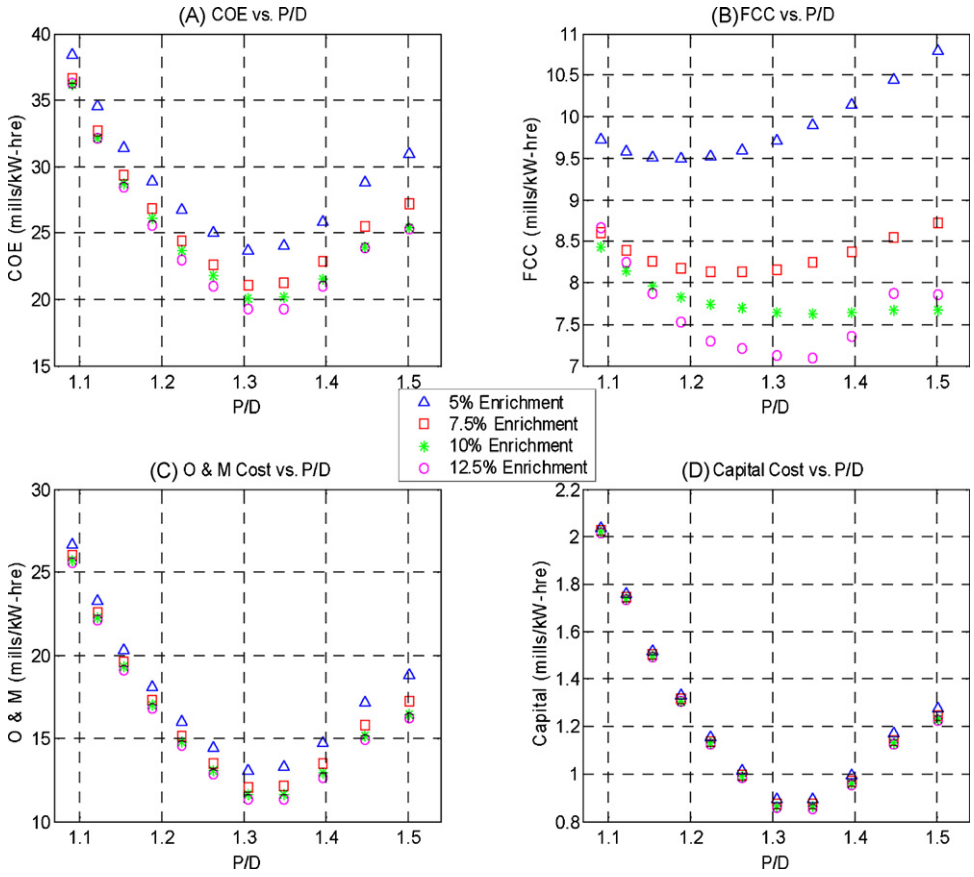

Fig. 16. Minimum COE and its components versus P/D for U–$ZrH_{1.6}$ at 0.20 MPa Minor Backfit scenario.

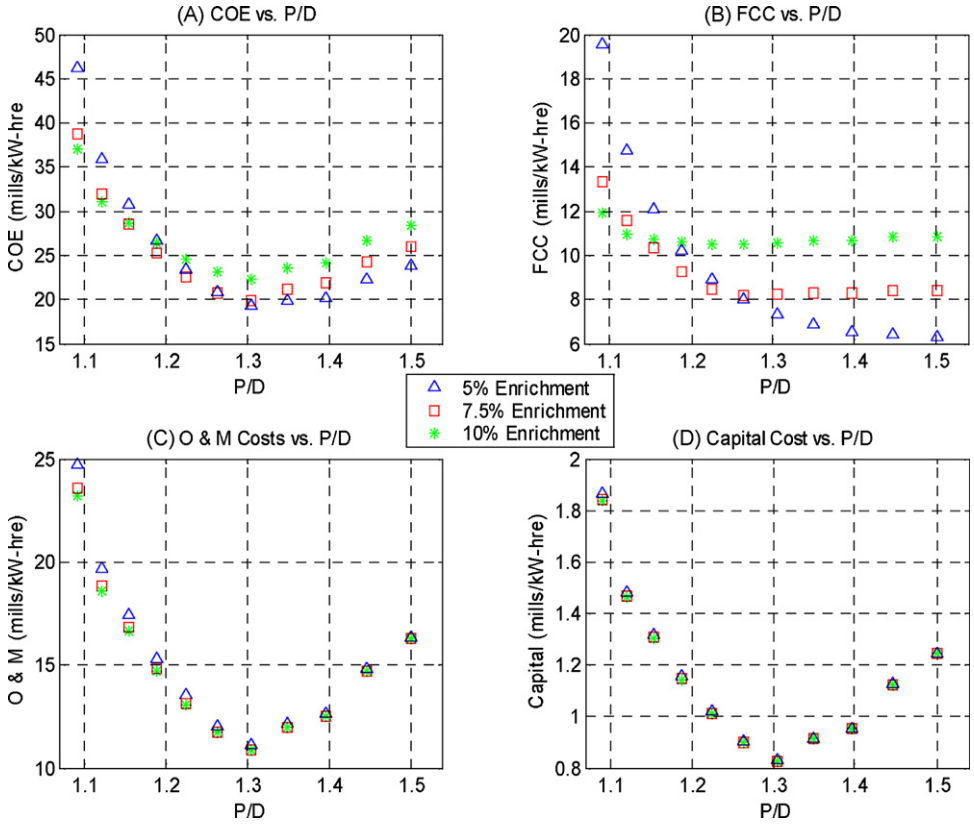

Fig. 17. Minimum COE and its components versus P/D for UO_2 at 0.20 MPa Minor Backfit scenario.

Please cite this article in press as: Greenspan, E., et al., Hydride fuel for LWRs—Project overview. Nucl. Eng. Des. (2009), doi:10.1016/j.nucengdes.2008.11.023

Table 5
Comparison of optimal and reference geometries for UO_2-fueled PWR cores.

Characteristic	0.20 MPa		0.414 MPa	
	Reference	Optimal[a]	Reference[b]	Optimal
COE (mills/kWh)	17.0	18.0[c]	22.2	18.0
Capital	0	1.3[c]	5.3	2.7
Fuel cycle	7.0	6.53	7.0	7.13
O&M	9.9	10.15	9.9	8.2
Power (MW_{th})	3,800	3,800	4,820[b]	4,820
Fuel rod outer diameter, D (mm)	9.5	7.13	9.5	6.5
P/D	1.326	1.47	1.326	1.39
Number of fuel rods	50,952	73,966	50,952	98,699
U inventory (kg_HM)	105,170	81,581	105,170	87,104
Linear heat rate (kW/m)	17.4	12.0	17.4	11.4
Power density (kW/l)	99.85	99.85	99.85	126.75
Specific power (kW/kg_{HM})	36.1	46.6	36.1	55.35
Average burnup (MWD/kg)	50.6	56.55	50.6	52.3
Cycle length (years)	1.35	1.17	1.35	0.9
Capacity factor	0.95	0.94	0.95	0.94
MDNBR	2.17	2.17	2.17	2.65
Peak fuel temp (°C)	1,482	1,041	1,482	1,026

[a] Optimal for a newly constructed PWR, not a retrofit;
[b] 3800 MW from the existing reference PWR plus 1020 MW from newly constructed 3800 MW PWR of the reference design.
[c] Capital cost component (and total COE) for a retrofitted PWR.

$D = 9.34$ mm. For UO_2, the minimum COE occurs at a similar geometry with the same cost: 19.3 mills/kWh at $P/D \sim 1.31$, $D = 9.66$ mm.

3.6. Discussion

The minimum COE of the hydride fuel designs identified above corresponds to designs that are somewhat over-moderated; their P/D exceeds 1.2. It is therefore assumed that 10% of the Zr of the hydride fuel is replaced by Th to assure a negative CTC. It is also assumed that this will not change the cost of the fuel, as the costs of Zr and Th are similar and the major cost component is that of the enriched uranium.

Under the set of constraints assumed in this work, hydride fuel was not found to offer any power density or economic advantage over oxide fuel in PWR cores when using fuel assembly designs featuring square lattice and grid spacers. This is because, contrary to our initial expectations, pressure drop constraints prevented achieving sufficiently high power using hydride fuel with a relatively small P/D ratio of around 1.2 or less, where it offers the highest reactivity and a higher HM loading. The attainable power density and economics of hydride fuel designs are expected to improve relative to those of oxide fuel with increase in the allowable pressure drop across the core. Alternatively, hydride fuel designs could be advantageous to oxide fuel for relatively small PWRs of limited fuel rod length, since for the same D, P, and coolant flow rate, the pressure drop is inversely proportional to the core height.

Another promising design approach for hydride-fueled PWRs involves use of a hexagonal lattice with wire wrap instead of the square lattice with grid spacers because the wire-wrap design approach features lower coolant friction losses in the design region of interest. This design approach is reviewed in Section 4.

As a spin-off of the comparison between hydride and oxide fuel performance, it was found that oxide-fueled PWR cores could be designed to have a significantly higher power density and lower COE than the reference design. Table 5 compares selected characteristics of a number of optimal UO_2 core designs identified in this work with the reference design. For the reference core pressure drop of 0.20 MPa in a square lattice with grid spacers, the lowest COE is obtained for 5%-enriched uranium at the reference geometry of $D = 9.5$ mm and $P/D = 1.326$. This is because the investment required for retrofitting the reactor to be able to accept a new core design, i.e., 1.3 mills/kWh (Fig. 15), more than offsets the lower attainable fuel cycle and O&M costs for other geometries. However, for a newly constructed 3800 MW_{th} PWR, the minimum COE will be obtained from a core having a significantly different geometry: $D = 7.13$ mm and $P/D = 1.47$; it is $[(7.0 + 9.9) - (6.53 + 10.15)]$ 0.22 mills/kWh smaller than the COE from the reference PWR (assuming the capital cost of the two new PWRs is the same).

If primary coolant pumps could be designed to provide a coolant pressure drop across the core of 0.414 MPa and the pressure vessel internals could accommodate it, the minimum COE is obtained for 5%-enriched fuel at the geometry: $D = 6.5$ mm; $P/D = 1.39$. The corresponding power density is 27% higher than the reference power density. The COE is estimated to be ~19% lower than the cost to achieve the same total power of 4820 MW from the reference core (3800 MW) supplemented by power purchased from a new 3800 MW PWR using the reference core design (1020 MW). The capital cost assumed for the newly constructed PWR is $1800/kW.

Relative to the reference core design, the optimal UO_2 core designs arrived at in this work feature smaller uranium inventory per core loading, larger number of fuel rods, shorter cycle length, smaller linear heat rate, significantly smaller peak fuel temperature, somewhat higher discharge burnup, and higher specific power.

A possible implication of the increased power density is that new PWRs could be designed for a significantly higher power, possibly up to ~2000 MW, than when using the contemporary core design geometry, without exceeding contemporary pressure vessel dimensions.

4. PWR – wire-wrapped hexagonal lattice designs

4.1. Introduction

The study presented in this section evaluates the relative merits of hydride and oxide fuel designs with hexagonal lattice having wire-wrap support instead of square lattice with grid-spacer support (Diller et al., this issue). Relative to square lattice, the hexagonal lattice can be designed to have a smaller coolant-to-fuel volume ratio – a feature that was expected to be of interest for hydride fuel that does not rely on the coolant as the sole moderator. The wire-wrap design has lower coolant pressure drop over most of the geometry range considered. This is illustrated for the reference fuel rod diameter, especially in the low P/D range in Fig. 18 (Diller et

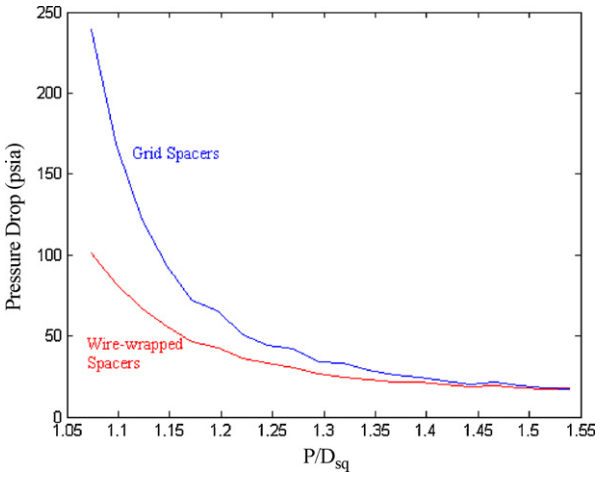

Fig. 18. Pressure drop comparison at reference power and pin diameter, wire lead equal to grid-spacer pitch.

al., this issue) – a feature that was also expected to be particularly beneficial for hydride fuel.

The scope of the study performed for the hexagonal lattice wire-wrapped design is similar to that of the square lattice grid-spacer design reported in Section 3. The study methodology was also similar, with the few exceptions described below. More details can be found in Diller et al. (this issue).

4.2. Methodology – general

The reference PWR reactor and the design variables used for this study are the same as used for the square lattice PWR design with grid spacers defined in Section 2. The range of pitch-to-diameter ratio considered is $1.15 \leq P/D_{wire} \leq 1.42$ where P/D_{wire} is the hexagonal wire supported geometry P/D; it is comparable to the range considered for the square lattice when expressed in terms of its thermal hydraulic equivalent as $P_{hex} = 1.0746\ P_{square}$. An additional design variable introduced in this study is the axial pitch, H. For grid spacers, H_{grid} is the reference core distance between spacers, and for wire wraps, H_{wire} is the axial distance over which the wire completely wraps around the rod. Due to the availability of data, all of the designs analyzed are single-start hexagonal wire-wrapped assemblies – historically by far the most common wire-wrap configuration.

Two scenarios were considered (Diller et al., this issue):

(a) Achievable case – corresponding to the conservative set of assumptions specified in Table 6.
(b) Stretch case – corresponding to more demanding constraints that are outside the range of experience but shows the potential advantages of wire wraps. Table 7 specifies these constraints.

The fuel rod gap is assumed to be filled with LM having a thermal conductivity of 35 W/m K – as assumed for the hydride fuel designs considered throughout this study.

Table 6
Steady-state achievable case constraints.

Constraint	Acceptable values	Calculated using
CHF	MDNBR > $MDNBR_{ref}$	W-3L correlation
Axial velocity	$V < V_{crit}$	Connors analysis
Peak fuel temperature (°C)	$T_{CL} < 750$	VIPRE
Clad temperature (°C)	$T_{Clad} < 350$	VIPRE
Coolant pressure drop (MPa)	<0.414	VIPRE
Wire-wrap axial pitch	H_{grid}	

Table 7
Steady-state stretch case constraints.

Constraint	Acceptable values	Calculated using
CHF	MDNBR > $MDNBR_{ref}$	Dalle Donne
Axial velocity	$V < V_{crit}$	Connors analysis
Peak fuel temperature (°C)	$T_{CL} < 750$	VIPRE
Clad temperature (°C)	$T_{Clad} < 350$	VIPRE
Coolant pressure drop (MPa)	<0.620	VIPRE
Wire-wrap axial pitch	0.75 H_{grid}	

4.3. Methodology – neutronics

The neutronic characteristics for the wire-wrapped hexagonal fuel assemblies were inferred from those calculated for the square lattice assemblies with grid spacers based on equivalency of the H/HM ratio for a given rod diameter, D (Diller et al., this issue). The methodology for the neutronic analyses for square lattice geometries is described in Section 2.4.

4.4. Methodology – thermal hydraulics

Grid spacers hold all of the rods together, while wire wraps only provide spacing. As a result, while bundle boxes are not necessary for PWR bundles with grid spacers, they are required with wire-wrap designs to hold the fuel rods together. Rather than closed bundle boxes as in BWRs, it is possible to use highly perforated box walls that will provide the needed mechanical support while enabling coolant cross mixing. Hence, open bundles as exist currently in PWRs were assumed in the subchannel mixing calculation.

Turbulent mixing with wire wraps is calculated using a correlation developed by Cheng and Todreas (Diller et al., this issue). The subchannel mixing is proportional to the gap size, $P - D$. Since VIPRE is run for square subchannels, the gap size and thus, the mixing coefficient, will be incorrect for the hexagonal subchannels but a separate study was performed to confirm that the core power was relatively insensitive to the mixing coefficient value.

For all of the wire-wrap CHF experiments examined in this study, the CHF performance of wire wraps was comparable to, or better than, grid-spacer performance (Diller et al., this issue). As a result, for the achievable case scenarios, the MDNBR was calculated using the W-3L correlation – identical to the approach used for the grid-spacer designs. This is the conservative approach.

Dalle Donne created the most commonly referred to wire wrap CHF correlation. This is a correlation for a spacer coefficient used in Bowring's WSC-2 CHF correlation. However, the WSC-2 correlation behaves differently than the W-3L correlation over the power map, and its direct application gave results inconsistent with previous results using the W-3L correlation. Consequently, at each geometry, the WSC-2 limit was found that allowed the same maximum power as predicted by the W-3L correlation for MDNBR of 2.17, guaranteeing consistent power maps with the two correlations. Dalle Donne's wire-wrap spacer coefficient was used in the WSC-2 correlation with the WSC-2 limit equivalent to the W-3L MDNBR limit of 2.17 (Diller et al., this issue). This is the best estimate approach of the stretch case.

The pressure drop was calculated using the Cheng–Todreas friction factor correlation for wire wraps (Diller et al., this issue).

The steady-state constraints applied are similar to those for the grid-spacers designs described in Section 2.5 and are summarized in Tables 6 and 7. An exception is the maximum allowable coolant pressure drop across the core assumed to be 0.620 MPa (90 psi) for the "stretch case" scenario.

4.5. Methodology – fuel rod vibrations

Two types of vibrations are considered – thermal hydraulic vibrations (THVs) and FIV. The Otsubo model was used for a

Please cite this article in press as: Greenspan, E., et al., Hydride fuel for LWRs—Project overview. Nucl. Eng. Des. (2009), doi:10.1016/j.nucengdes.2008.11.023

conservative analysis of THV (Diller et al., this issue); these are low-frequency vibrations caused by feedback between the fluid flow and rod bow due to thermal expansion in the fuel rods. An empirical equation for the critical cross-flow velocity of a rod bundle pinned at both ends derived by Connors was used for the analysis of FIV (Diller et al., this issue) – high-frequency vibrations caused by local pressure variations due to the nature of the turbulent flow. The cross-flow velocity was calculated for each geometry from the axial-flow velocity using the sweep angle of the wire wraps, so that the FIV limit was effectively a limit on the axial velocity.

Fretting wear is a significant concern when implementing wire wraps, because the wires of one rod directly contact the adjacent rod. Shuffler et al. (2006) (also Section 2.7) calculated the total fretting wear for gridded arrays over the fuel cycle length and constrained this to be less than the reference core total fretting wear. The fretting wear rate was calculated for the reference geometry at the reference power. This was done using grid spacers and wire wraps, and the wire-wrap fretting wear rate was found to be 10.4% lower than the grid-spacer fretting wear rate. This is promising, but fretting wear experiments are needed perhaps more than any other type of experiment to verify wire-wrap performance.

4.6. Methodology – clad integrity

Although the clad integrity imposed limit on the attainable burnup depends on the attainable hot-rod power, no self-consistent fuel performance analysis was performed for wire-wrap designs. Instead, the burnup map created for the 0.414 MPa grid-spacer designs and reported in Section 3.3 was assumed applicable for the wire-wrap designs; the power levels of the wire-wrap designs are closest to those of the 0.414 MPa grid-spacers designs. The methodology used for the clad integrity analysis is described in Section 2.6.

4.7. Methodology – economics

The economic analysis methodology used is similar to that described in Section 2.9. Due to the inherent fuel assembly geometry change required to accommodate the hexagonal lattice of wire-wraps rods, Minor Backfit scenarios are not possible for wire-wrap designs; consequently, the economic analysis is performed only for Major Backfit scenarios.

4.8. Results – steady-state

Fuel temperature is the only limit that depends on fuel type. However, the fuel temperature limits are not constraining for regions of maximum power. Consequently, the steady-state achievable power for hydride and oxide fuel designs is almost identical, and in practice is identical for the regions of maximum power.

A 64.5% power increase over the reference core is obtained for the achievable case (6251 MW_{th}), and 88.3% for the stretch case (7156 MW_{th}). The achievable case maximum power geometry is $D = 8.39$ mm, $P/D_{wire} = 1.42$. The latter is equivalent to $P/D_{sq} = 1.321$. The stretch case preferable geometry is $D = 8.71$ mm with $P/D_{wire} = 1.42$. While the power at the preferable geometry is very slightly lower than the maximum attainable, the preferable geometry has a larger fuel rod diameter that is closer to the reference diameter.

4.9. Results – transient analysis

The transient performance of wire wraps was analyzed for the overpower transient and the LOCA; as reported in Section 3.4, loss-of-flow accidents were found not to limit the attainable power of square lattice designs. The overpower transient was evaluated using the MATLAB/VIPRE interface, analogous to the steady-state analysis (see Sections 2.5 and 2.7). The only difference is that the average LHGR of the core is increased by 17.3%, the stated overpower value of the reference core. The MDNBR of the reference core is recalculated with the new linear heat rate, and is taken as the new MDNBR limit for the overpower transient. This new MDNBR limit is more constraining than the steady-state MDNBR limit and the axial velocity is generally higher as well. As a result, the achievable powers of the overpower transient are lower than those of the steady-state by 3.6% for the achievable case and 5% for the stretch case. As for the steady-state analysis, the hydride and oxide power maps are essentially identical.

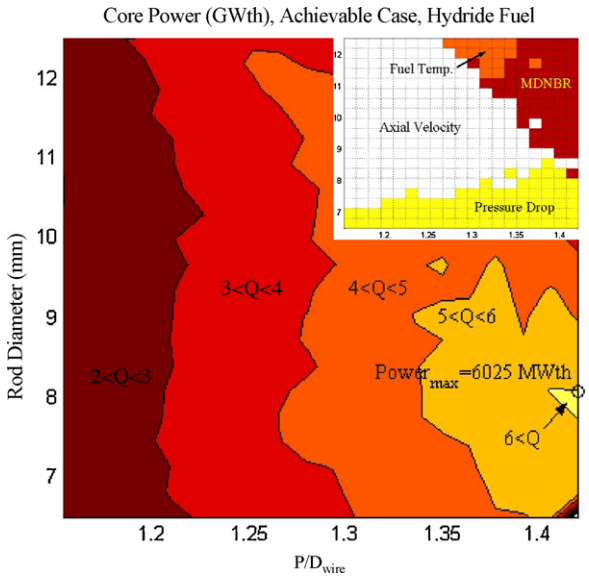

Fig. 19. Achievable case hydride power map accounting for transients.

The LOCA performance of wire wraps was calculated using RELAP 5-3D for both hydride and oxide fuels. The constraining limits were found to be the cladding temperature of 1204 °C for oxide fuel and the fuel temperature of 1050 °C for hydride fuel. The LOCA analysis was only performed for the achievable case maximum power geometry. The safety injection (SI) system was assumed to scale with the power, allowing the core to eventually cool, even for power uprates on the order of 100%. It was found that the power predicted using steady-state analysis for the achievable case scenario is within the limits for both of the fuels, while both of the fuels exceed their design limits for the stretch case scenario.

Figs. 19 and 20 give the attainable power as calculated using, respectively, the achievable case and stretch case scenarios, accounting for the overpower transient and LOCA. The maximum power of the stretch case, 6251 MW_{th}, is only 4% higher than the maximum power of the achievable case – 6025 MW_{th}. Considering the liberal assumptions applied to the stretch case, this marginal increase in power obviates any benefits from further consideration of the stretch case. Hence, the maximum power of a wire-wrapped hexagonal lattice design is taken to be 6025 MW_{th} – a 59% power increase over the reference core.

4.10. Results – burnup limits

The burnup limits used for the economic analysis are the smaller of the values determined by the neutronic analysis (Section 4.3) and by the clad integrity analysis (Section 4.6). Figs. 21 and 22 give the reactivity limited burnup maps for hydride and oxide fuels with 12.5 and 7.5% enrichments, respectively. These enrichments were found to have the lowest COE in the economic analysis. The clad integrity

Please cite this article in press as: Greenspan, E., et al., Hydride fuel for LWRs—Project overview. Nucl. Eng. Des. (2009), doi:10.1016/j.nucengdes.2008.11.023

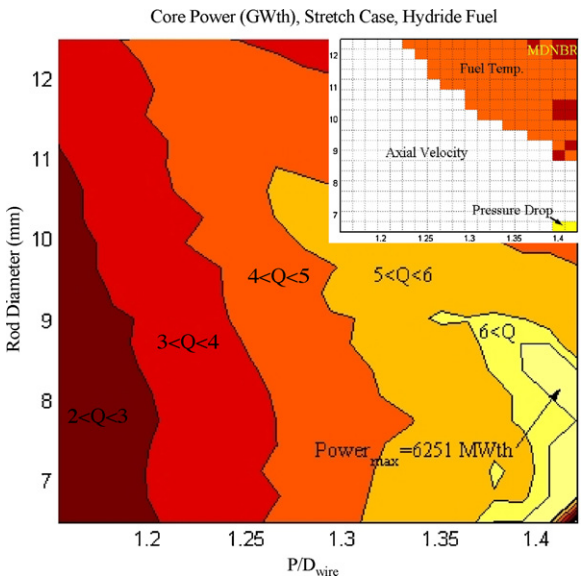

Fig. 20. Stretch case hydride power map accounting for transients.

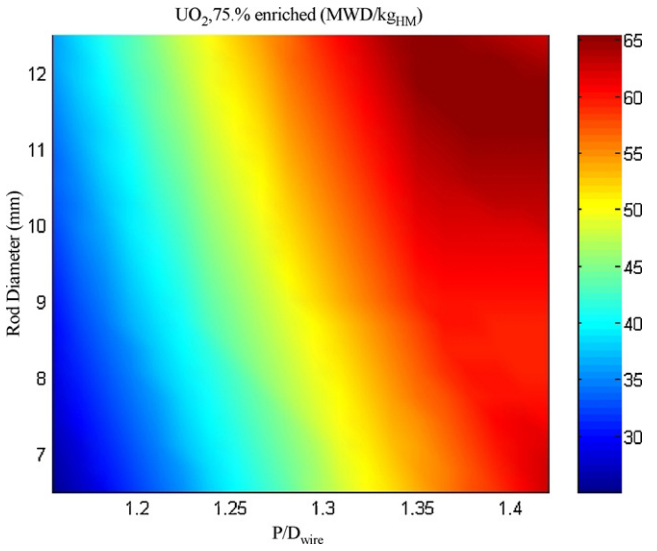

Fig. 22. Reactivity-limited burnup for 7.5% UO_2 wire-wrapped lattices.

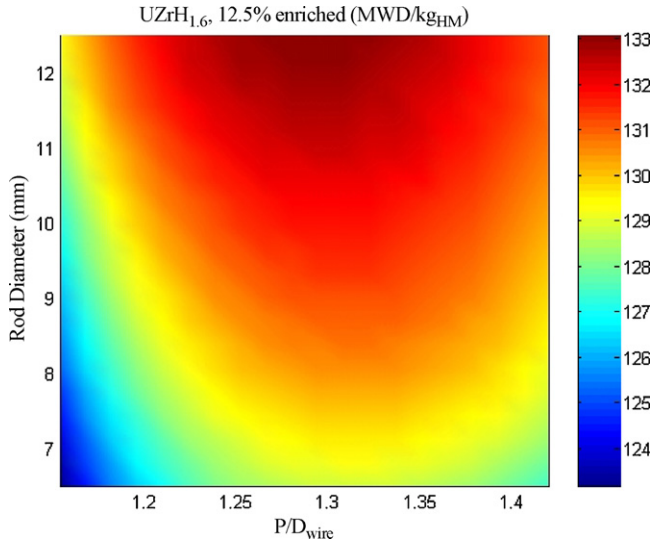

Fig. 21. Reactivity-limited burnup for 12.5% U–$ZrH_{1.6}$ wire-wrapped lattices.

limited burnup values were found (Romano et al., this issue) generally less constraining than the reactivity limited burnups.

4.11. Results – economics

The economic analysis was performed over all of the geometries considered for oxide and hydride fuels. Table 8 summarizes the findings for optimal wire-wrap designs and compares them against the optimal grid-spacers designs reported in Section 3.5. All cases are for cores that fit in the reference plant reactor vessel. The three Major Backfit cases use new fuel assembly envelopes and control rod layouts, thus requiring new vessel heads and internals as well as larger primary loop components for the increased power ratings. The wire-wrap results given in Table 8 pertain to the final power map; i.e., they account for all the constraints, including the transient constraints.

It is found that the achievable case, the most conservative hydride fuel wire-wrap design, has a COE of 17.11 mils/kWh. It is lower than the COE of all the grid-spacer design alternatives, with the exception of the reference oxide plant. The minimum COE of the oxide core design, not shown in the table, was found to be 0.7 mils/kWh higher than that of the hydride core design pertaining to the same scenario.

Table 8
Comparison of grid spacer and wire wrap designs with optimal fuel type and enrichment.

	Reference plant	Major Backfit			No Backfit
		Grid spacers Grid spacer uprate	Wire wraps, final power Achievable case	Stretch case	1.58 Reference plants
Fuel type	UO_2	UO_2	$UZrH_{1.6}$[a]	$UZrH_{1.6}$[a]	UO_2
Enrichment (%)	5	5	12.5	12.5	5
Fuel rod OD (mm)	9.5	6.5	8.08	8.71	9.5
P/D_{actual}	1.326	1.39	1.41	1.39	1.326
Linear heat rate (kW/m)	17.4	11.4	19.8	25.6	17.4
Power (MW_{th})	3800	4820	6011	6251	6011
Power increase (%)	–	27	58.18	64.50	58.18
Capacity factor	0.95	0.94	0.94	0.94	0.95
Cycle length (years)	1.35	0.9	0.90	0.90	1.35
COE (mils/kWh)	17.0	18.0	17.11	16.73	26.23
Fuel cycle cost	7.0	7.1	7.63	7.49	7.0
O&M cost	9.9	8.2	6.65	6.39	9.9
Capital cost	0	2.7	2.83	2.85	9.23

[a] The COE of oxide was found an average of 4% or 0.7 mils/kWh higher than hydride for the same case.

Please cite this article in press as: Greenspan, E., et al., Hydride fuel for LWRs—Project overview. Nucl. Eng. Des. (2009), doi:10.1016/j.nucengdes.2008.11.023

The "1.58 reference plants" case of Table 8 is the reference against which the achievable case wire-wrap design is to be compared with – it consists of one reference plant (as of the rightmost column of Table 8) plus 58% of a new reference-like plant that needs to be constructed in order to provide a combined power of 6011 MW_{th} that is comparable to the power attainable from the backfit "achievable case". The FCC and O&M COE are the same as for the reference plant, but the new reference plant capital cost is charged \$1800/kW for the 58%, i.e., 2211 MW_{th}, of its rated energy. It is found that the wire-wrap Major Backfit design approach offers ~40% lower COE than construction of a new reference plant to provide the same total power – 17.11 mils/kWh versus 26.23 mils/kWh.

4.12. Discussion

While any shift from the use of square lattices with grid spacers to hexagonal lattices with wire wraps would require a major development and major retrofitting, the potential performance advantages of wire-wrap designs justify their further investigation. The most notable advantage of wire wraps over grid spacers is their significant improvement in pressure drop and CHF. Contrary to intuition, wire wraps could also provide improved vibrations characteristics – wire wraps do not relax with radiation exposure and provide support at many more axial locations, thus improving both the fretting wear and FIV performance. Neither FIV nor fretting has ever been observed in wire-wrap testing.

The reduced pressure drop of wire-wrap designs enables significant increases in the power density attainable from PWR cores and, thereby, significant improvement in their economics. The power density increase and COE attainable with hydride fuel are comparable to those also attainable with oxide fuel. The fuel rod outer diameter and lattice pitch of the optimal wire-wrap designs found are in the range of D = 0.8–0.9 mm and P/D slightly larger than 1.4.

5. PWR – inverted geometry designs

5.1. Introduction

The proposed inverted geometry for hydride fuel is composed of hexagonal blocks of fuel (referred as "assemblies") perforated by non-communicating cylindrical coolant channels, similar to the fuel concept proposed for gas-cooled fast reactors (Pope et al, 2005). A cylindrical Zircaloy clad lines the wall of each coolant channel, and a LM-filled gap separates the outer clad surface from the inner surface of the fuel. As shown in Fig. 23, while for standard rod bundles, the subchannel is a coolant channel surrounded by circular fuel rods, for the inverted design, the subchannel is a circular coolant channel surrounded by a hexagonal fuel cell. The circular channels are arranged within the fuel in hexagonal close-packed arrays to minimize the conduction length between the channel wall and the boundary of the fuel subprism. They are only connected at the core inlet and outlet, where flow distribution is determined. Twisted tape inserts may be attached to the inner wall of the channels to enhance the critical heat flux at the expense of added pressure drop. A preliminary investigation of the performance of the inverted geometry with and without twisted tapes was performed (Malen et al., this issue).

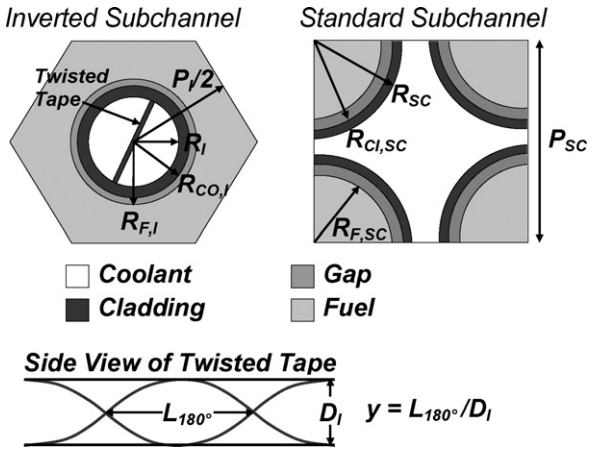

Fig. 23. Comparison of inverted and standard subchannels.

The incentive for the inverted geometry is to increase the fuel volume fraction in the core so as to compensate for the relatively low uranium density of hydride fuel. Hydride fuel is more suitable for the inverted design than oxide fuel because (a) its neutronically optimal coolant-to-fuel volume ratio is smaller than for oxide fuel and (b) it can be more easily fabricated into inverted fuel assemblies by casting the U–Zr metal and then hydrating it.

The number and height of inverted subchannels within each assembly, and the number of assemblies in the core may vary. This study does not address the optimization of these core characteristics since it analyzes the thermal hydraulic performance of a single subchannel, from which whole core properties such as HM loading and total power are obtained by means of geometric relations and conservative assumptions regarding the core radial power distribution. The subchannel geometry is however not constant since the cooling channel diameter and the pitch are varied in search of the optimally powered design.

5.2. Methodology

The goal of this study was to obtain a preliminary estimate of whether the COE could be reduced using U–$ZrH_{1.6}$ fuel in the inverted design. For comparison, three designs, all utilizing U–$ZrH_{1.6}$ fuel, were studied:

1. standard (pin-geometry) core (SC),
2. inverted core (IC),
3. inverted core with twisted tape (ICTT) inserts.

All three cores are 3.66 m tall and occupy the same volume.

A parametric study over a range of geometries was completed to identify the optimal combination of pitch and diameter for each of the three designs. It is useful to define the geometry, hitherto defined by pitch and diameter, in terms of fuel area per subchannel (AF) and fuel-to-coolant volume ratio (FCR). These variables enable a direct comparison of the standard and inverted designs, even though their subchannel geometries are reversed. Furthermore, neutronic performance is highly dependant on FCR, so it is appropriate to compare standard and inverted designs of equivalent FCR.

The maximum achievable power of each design (SC, IC, and ICTT) was determined for a range of geometries. The maximum achievable power of a given geometry is defined as the highest steady-state power that can be sustained without exceeding a single constraint limit. The constraints considered include fuel temperature and cladding temperature during steady-state operation, and minimum departure from nucleate boling ratio (MDNBR) during an overpower event. Together with the overpower transient, the LOCA was also considered because it further limits steady-state core power. A coolant velocity constraint, which was applied to the SC design to limit flow-induced vibrations, was not applied to IC and ICTT designs since they are assumed to inherently resist vibrations. Further studies are needed to assess the structural stability of the twisted tape under the effect of high-coolant velocity. Although core pressure drop is a realistic limitation, it is not a safety concern with a hard upper limit. Hence, a pressure drop constraint was not

Please cite this article in press as: Greenspan, E., et al., Hydride fuel for LWRs—Project overview. Nucl. Eng. Des. (2009), doi:10.1016/j.nucengdes.2008.11.023

Table 9
Comparison of inverted geometry designs.

Comparison case	Design	D[a] (mm)	P/D	Power[b] (MW_{th})	Specific power (kW/kg_{HM})	T_{cycle}[c] (months)	ΔP (MPa)	V (m/s)	T_{max}[d] (°C)
(A) Unconstrained geometry – max. power	SC	5.89	1.42	5080	162.7	9.6	0.36	7.8	517
	IC	10.12	1.14	4246	169.7	8.7	0.09	5.7	390
	ICTT $y = 5.0$	12.87	1.14	6044	241.6	6.1	0.23	8.1	449
	ICTT $y = 2.5$	13.92	1.14	6869	274.5	5.4	0.33	9.2	482
	ICTT $y = 2.5\ D^{-1/3}$	13.04	1.14	6334	253.1	5.8	0.32	8.5	456
(B) Unconstrained geometry – match SC max. Power FCR	IC	9.70	1.22	4055	129.9	12.0	0.11	6.3	407
	ICTT $y = 5.0$	12.19	1.22	5660	181.3	8.6	0.28	8.7	480
	ICTT $y = 2.5$	13.26	1.22	6440	206.3	7.6	0.41	9.9	527
	ICTT $y = 2.5\ D^{-1/3}$	12.49	1.22	5970	191.2	8.2	0.40	9.2	496
(C) Unconstrained geometry – match SC max Power	ICTT $y = 5.0$	11.17	1.35	5080	126.0	12.6	0.38	9.6	528
	ICTT 2.5	11.14	1.53	5080	102.5	15.3	0.76	12.2	665
	ICTT $y = 2.5\ D^{-1/3}$	11.12	1.44	5080	111.4	14.2	0.63	11.0	595
(D) Constrained geometry – conservative fuel dimensions	ICTT $y = 2.5$	13.26	1.30	5812	181.5	8.7	0.45	9.8	616
	ICTT $y = 2.5\ D^{-1/3}$	13.26	1.30	5062	158.1	10.0	0.35	8.6	582
	ICTT $y = 2.5$	13.26	1.38	5250	130.2	12.2	0.46	9.9	655
	ICTT $y = 2.5\ D^{-1/3}$	13.26	1.38	4500	111.6	14.3	0.35	8.5	612

[a] D for SC is the rod diameter, while D for IC and ICTT is the channel diameter.
[b] For the inverted geometry, an inter-assembly gap spacing of 5 mm and an assembly external clad of 4 mm, not modeled in this analysis, will reduce the power by about 10%.
[c] Cycle length calculated assuming three-batch refueling strategy and capacity factor of 0.9, with BU for 12.5%-enriched U–$ZrH_{1.6}$ (Ganda and Greenspan, this issue)
[d] T_{Max} is the maximum fuel temperature in the core (the peak temperature of the hot rod at centerline for the SC).

applied, although the technical feasibility of the derived pressure drop for each design will be discussed.

5.3. Thermal hydraulic results

Core power as a function of FCR is shown in Fig. 24; the bracketed quantities in the abscissa label are the associated P/D ratio for the inverted and standard designs. For the ICTT designs, y is the axial length required for the twisted tape to complete 180° twist, per unit channel internal diameter (see Fig. 23), and $D^{-1/3}$ refers to an alternative diameter dependence of the twisted tape CHF correlation. The SC curve peaks at 5080 MW_{th} for an FCR of 0.5, corresponding to P/D of 1.4. The peak powers of the IC, ICTT $y = 2.5$, ICTT $y = 2.5\ D^{-1/3}$ and ICTT $y = 5.0$ all occur at the smallest FCR considered (FCR = 0.3) and are 4246, 6869, 6334, and 6044 MW_{th} respectively. The addition of twisted tape significantly enhances the achievable power due to increased CHF. Reducing y increases CHF and the achievable power, but causes increased pressure drop. These general conclusions regarding twisted tape inserts are still valid, given the more conservative $D^{-1/3}$ CHF dependence.

The core pressure drops, flow velocities and fuel temperatures associated with the powers of Fig. 24 are plotted as a function of FCR in Malen et al. (this issue).

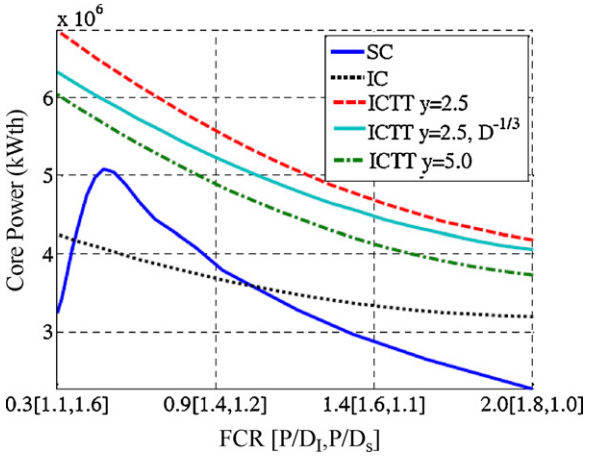

Fig. 24. Core power versus fuel to coolant ratio for SC, IC, and ICTT designs.

5.4. Geometries of economic interest

Rather than searching for the specific geometry of the IC design that gives the minimum COE as done by Shuffler et al. (this issue-b), the approach used to assess the economic viability of the inverted design was to identify the range of inverted designs that will concurrently outperform the hydride SC in core power, fuel burnup, and HM loading. Geometries of economic interest were grouped into the following comparison cases:

(A) unconstrained geometry; comparison of maximum power.
(B) unconstrained geometry; comparison of inverted geometries with equivalent FCR to that of the maximum power SC geometry.
(C) unconstrained geometry; comparison of inverted geometries with equivalent power to that of the maximum power SC geometry.
(D) constrained geometry; conservative fuel dimensions.

Case (D) has constrained fuel dimensions to provide a preliminary estimate of the inverted geometry performance when manufacturability and mechanical load constraints are considered. Specifically, minimum fuel web thicknesses t_{web}[10] of 2 and 3 mm were considered to represent probable and worst case scenarios. Conservative limits, detailed in Malen et al. (this issue), were also placed on the clad and gap thicknesses in case (D). The unconstrained geometries (cases A–C) have no minimum limitation on these parameters. Table 9 summarizes the geometry, thermal hydraulic performance parameters, and economic performance parameters of cases (A)–(D).

For comparison (A), the ICTT geometries clearly offer higher power and specific power than the SC, but a concurrent reduction in cycle length. Core pressure drops of the highest power cases are similar to the SC, which is 0.36 MPa, but 65% higher than the reference oxide SC (0.20 MPa). Maximum fuel temperatures are well below the 750 °C limit.

For comparison (B), the FCR, BU, and HM mass of the inverted geometries are the same as the maximum powered SC, but power increases are only attainable by the ICTT geometries. Cycle lengths

[10] defined from Fig. 23 as $t_{web} = P_I - 2R_{FI}$ (Malen et al., this issue).

Please cite this article in press as: Greenspan, E., et al., Hydride fuel for LWRs—Project overview. Nucl. Eng. Des. (2009), doi:10.1016/j.nucengdes.2008.11.023

are short, but the ICTT geometries of case (B) offer significant power upgrades relative to the SC, with acceptable maximum fuel temperature and pressure drops ranging between −27 to +14% with respect to the SC.

For comparison (C), the power of the inverted geometries is taken the same as the maximum powered SC, but the ICTT geometries offer increased FCR, BU, and HM mass. Resulting specific power values are lower than for the SC, while cycle lengths are higher due to increased fuel loading. Fuel temperatures are again acceptable. The pressure drop requirements of the ICTT $y = 2.5$ and ICTT $y = 2.5\ D^{-1/3}$ designs may be prohibitive if development of pumping technology requires significant capital investment.

For comparison (D), the 2 mm web thickness ICTTs exhibit significant power increases relative to the SC if the twisted tape CHF does not have a $D^{-1/3}$ dependence. Its cycle length and pressure drop are comparable to that of the SC. The 3 mm web thickness ICTTs offer higher power and longer cycle length than the SC, given that CHF does not have a $D^{-1/3}$ dependence. Fuel temperatures are high but acceptable.

5.5. Conclusions

The thermal hydraulic performance of U–$ZrH_{1.6}$-fueled IC designs with and without twisted tape were estimated and compared to those of the standard rod bundled core design also fueled with U–$ZrH_{1.6}$. Neutronic feasibility of the inverted design was not established. It was found that ICs without twisted tape do not offer power upgrades relative to the standard design. The use of twisted tape increases the CHF of the inverted design and thereby permits higher steady-state core powers than can be realized by the standard design. Higher power, burnup, and HM loading can be concurrently achieved by the IC with twisted tape relative to the optimal SC. The power of the current optimal inverted design with twisted tape, which has fuel web and clad thickness just below our acceptable ranges, is 6870 MW_{th}, which is 135% of the optimally powered U–$ZrH_{1.6}$ standard design (5080 MW_{th}). This may imply potential economic advantages for IC designs. Upon design optimization using reasonable values for fuel web and clad thickness, we expect the inverted design power to be slightly reduced. Future work necessary to confirm the performance capabilities and cost benefits of the inverted design is identified in Malen et al. (this issue).

6. PWR – plutonium-containing designs

6.1. Introduction

A drawback of the hydride fuel considered so far is that, due to its relatively low HM density, it requires higher enrichment than oxide fuel to provide the reference PWR cycle length and to minimize the COE. However, if the primary fissile material is Pu, as is the case if the PWR is to recycle Pu, the low HM inventory of hydride fuel is, in fact, an advantage, as is the enhanced moderation due to the hydrogen incorporated in the fuel. The primary objective of the work reported in this section (Ganda and Greenspan, this issue) is to compare the transmutation capability of the PWR that is fueled with uniform fuel assemblies using either hydride or MOX fuel. This capability is measured by the fraction of Pu that is transmuted per cycle and by the radiotoxicity, neutron source strength, and decay heat of the discharged fuel. Being a preliminary feasibility assessment, only neutronic analysis was performed (Ganda and Greenspan, 2005a, b, this issue). It is assumed that the thermal hydraulic performance of the Pu-bearing fuel will be comparable to that of the enriched uranium fuel considered above.

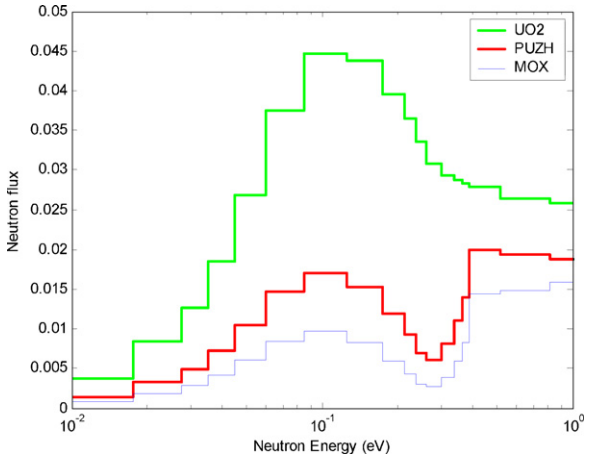

Fig. 25. BOL thermal neutron spectrum (per unit lethargy) in the fuel. Normalized to one over the full range $0 < E < 10$ MeV (only portion shown).

If MOX fuel is used to replace all of the UO_2 in the reference PWR fuel assembly geometry, this core neutron spectrum is significantly harder than that of the reference UO_2 core, as illustrated in Figs. 25 and 26. This relatively hard neutron spectrum impairs the achievable discharge burnup and fractional transmutation of Pu per cycle, reduces the reactivity worth of the control and safety rods as well as of the soluble boron, and due to positive void coefficient, limits the number of possible recycles. Consequently, many fuel assemblies designed for Pu recycling feature higher water-to-fuel volume ratio than in the reference UO_2-fueled PWRs, as can be found in references cited in Ganda and Greenspan (2005a, b, this issue).

MOX-containing fuel assemblies that offer acceptable performance, like the so-called "CORAIL" design or "CONFU" design are highly heterogeneous (Youinou et al., 2001; Taiwo et al., 2003; Shwageraus et al., 2003). Other designs include addition of moderator at the expense of fuel volume (Trellue, 2004), thereby softening the neutron spectrum and improving the destruction efficiency and safety features of the core but also reducing the attainable power level and impairing the PWR economics.

Hydride fuel offers a number of new possibilities for loading Pu (and MA, these were not considered in the present work) into PWRs. The hydride fuel we are proposing as the direct equivalent to MOX fuel is U–PuH_2–$ZrH_{1.6}$ (PUZH) fuel. When loaded into the reference PWR fuel assembly, it gives a significantly softer spectrum than MOX fuel assembly designed to generate the same amount

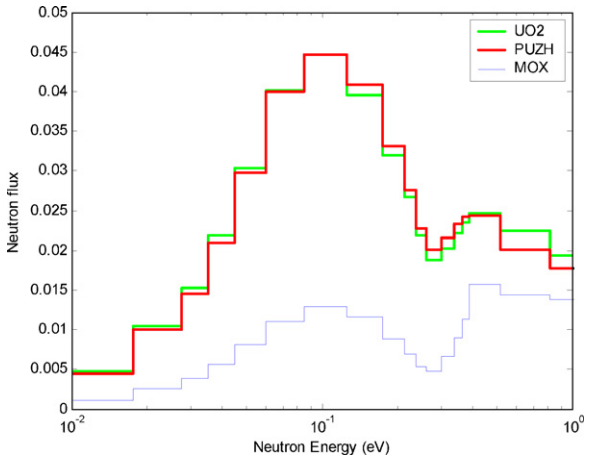

Fig. 26. EOL thermal neutron spectrum (per unit lethargy) in the fuel. Normalized to one over the full range $0 < E < 10$ MeV (only portion shown).

Please cite this article in press as: Greenspan, E., et al., Hydride fuel for LWRs—Project overview. Nucl. Eng. Des. (2009), doi:10.1016/j.nucengdes.2008.11.023

Table 10
Specifications of the reference unit cell.

	PUZH	MOX
Fuel diameter (cm)	0.8205	0.8192
Clad inner diameter (cm)	0.8357	0.8357
Clad outer diameter, *D* (cm)	0.95	0.95
Lattice pitch, *P* (cm)	1.26	1.26
P/*D*	1.326	1.326
Specific power (W/g iHM)	76.72	36.14
Linear heat rate (W/cm of rod)	176.53	176.53
Equivalent lattice *P*/*D*	1.393	1.393

of energy due to the larger hydrogen-to-Pu (and also H-to-HM) ratio of the hydride fuel. Fig. 25 shows that the spectrum at BOL is between that of MOX and that of the UO_2-fueled PWR. At end of life, shown in Fig. 26, the neutron spectrum is even softer than that of the reference PWR because of the significant consumption of Pu, that increases the H/HM ratio.

The amount of Pu loaded into the MOX and PUZH fuel referred to in Figs. 25 and 26 is that required to make their cycle length similar to the 18-month cycle of the reference UO_2-fueled PWR in a three-batch fuel management. The latter uses 5%-enriched U.

A potential difficulty of hydride fuel is the separation of the zirconium from the actinides in case recycling of actinides is of interest. We did not study this issue in the present project.

6.2. Methodology

A scoping study was first performed covering the following design space (Ganda and Greenspan, 2005a, b, this issue): clad outside diameters, *D*, ranging from 0.65 to 1.25 cm and lattice pitch-to-diameter ratio, *P*/*D*, ranging from 1.05 to 2.0. For each of these geometries (77 in total) the achievable three-batch burnup and the reactivity coefficients along the fuel life were calculated. A "feasibility map" was then constructed for each fuel type based on the requirement that a geometry is feasible only when all the reactivity coefficients (averaged over the three batches) are negative at any time during the cycle. The study then focused on the reference PWR unit cell geometry and made a detailed comparison of the Pu recycling capabilities of PUZH versus MOX fuel. This latter comparison is described below.

The reference PWR unit cell dimensions and specific power are summarized in Table 10. The Pu composition assumed for BOL is typical of the Pu discharged from PWR; it consists of 1, 61, 24, 9, and 5 at% of, respectively, ^{238}Pu, ^{239}Pu, ^{240}Pu, ^{241}Pu, and ^{242}Pu. The amount of Pu loaded into MOX and PUZH fuels is adjusted to give the same cycle length as of the reference 5%-enriched UO_2 PWR with all cores assumed to operate at the same unit cell linear heat rate. Table 11 gives the MOX and PUZH fuel initial compositions. The methodology used for the neutronic analysis of Pu-bearing PWR fuels is the same as that described in Section 2.4. For all three fuel types considered, the burnup-dependent excess reactivity is compensated for by adjusting the soluble boron concentration in the water. In case of the UO_2 fuel, IFBA is also used to compensate for the excess reactivity; otherwise the BOC CTC is positive.

Table 11
Initial composition (atoms/barn-cm) of MOX and PUZH fuels.

Isotope	MOX	PUZH
U-235	5.352E-05	2.353E-05
U-238	2.136E-02	9.390E-03
PU-238	2.021E-05	1.714E-05
PU-239	1.233E-03	1.046E-03
PU-240	4.850E-04	4.113E-04
PU-241	1.819E-04	1.543E-04
PU-242	1.010E-04	8.570E-05
Tot U	2.141E-02	9.414E-03
TOT Pu	2.021E-03	1.714E-03
Pu atom fraction (%)	2.343E-02	1.113E-02

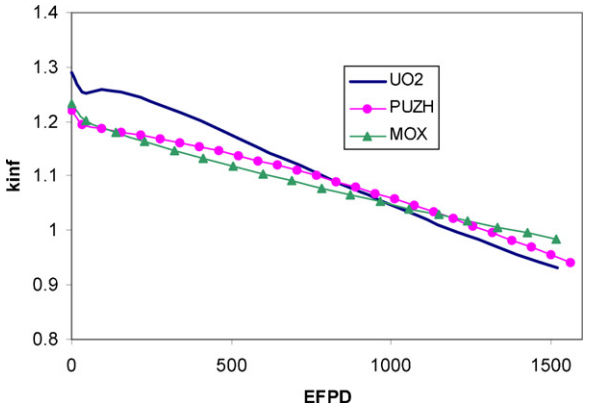

Fig. 27. k_∞ evolution with cycle time for PUZH and MOX fuels versus UO_2 fuel in the reference PWR geometry, all giving same discharge burnup.

6.3. Results

Fig. 27 compares the k_∞ evolution of the PUZH and MOX-fueled unit cells designed to provide the same cycle length as the reference 5%-enriched UO_2 unit cell also shown in the figure. It is found that the PUZH-fueled lattice has very similar burnup-dependent k_∞ as that of the reference UO_2-fueled lattice, whereas the MOX-fueled lattice has a flatter k_∞ evolution as a result of a higher conversion ratio.

Four reactivity coefficients were calculated for the PUZH system; those associated with fuel temperature, coolant temperature, small-coolant voiding, and large-coolant voiding. They were all found to be negative for the PUZH-fueled system.

Selected transmutation characteristics of the PWR fueled with PUZH are compared in Table 12 against that of a full-MOX-fueled PWR of the reference PWR geometry at 1 year after discharge. It is found that for the same cycle length (1512/3 = 504 EFPD) at the same linear heat rate (176.5 W/cm), the PUZH fuel requires 15% less Pu loading and 56% less depleted uranium loading than the MOX fuel and achieves more than double the average discharge burnup – 114.61 GWD/*t*HM versus 54.66 GWD/*t*HM of MOX. This high burnup is close to the 120 GWD/MTiHM routinely achieved by TRIGA fuel (Olander et al., this issue). The net amount of Pu consumed per cycle is 55% higher in cores using PUZH than in cores using MOX fuel. This is due to the smaller initial Pu inventory and to the lower conversion ratio of the PUZH core: the ratio of neutron capture rate in ^{238}U to

Table 12
Selected transmutation characteristics of PUZH and MOX fuels.

Characteristic	MOX	PUZH
Burnup (GWD/*t*)	54.7	114.6
Residence time (EFPD)	1512	1511
Discharged Pu inventory (g/cc)	0.573	0.324
Discharged/initial Pu inventory	0.713	0.475
% Pu incinerated/cycle	28.7	52.5
Fissile Pu/total Pu (%)	60.3	45.5
MA inventory (g/cc)	0.0340	0.0341
MA/Pu at discharge (%)	6.98	10.54
Neutron source (n/s/cc)	8.64×10^4	8.93×10^4
Activity (Ci/cc)	12.28	9.10
Decay heat (w/cc)	0.0797	0.0820
Neutrons per g Pu (n/s)	561	825
Neutrons per g HM (n/s)	9.87×10^3	2.30×10^4
Specific heat (w/g Pu)	0.015	0.021
Specific heat (w/g HM)	0.0091	0.0211

Please cite this article in press as: Greenspan, E., et al., Hydride fuel for LWRs—Project overview. Nucl. Eng. Des. (2009), doi:10.1016/j.nucengdes.2008.11.023

Table 13
Selected transmutation characteristics of PuH_2–ThH_2 and MOX-fueled cores.

Characteristic	PuTh–H	MOX
Burnup (GWD/t)	64	54.66
Residence time (EFPD)	1,814	1,512.45
Discharged Pu inventory (g/pin)	68.5	115.0
Discharged/initial Pu inventory	0.375	0.713
% Pu incinerated/cycle	62.5	28.7
Fissile Pu/total Pu (%)	43	60
MA inventory (g/pin)	8.95	7.77
MA/Pu at discharge (%)	13	6.98
Neutron source (n/s/pin)	36.1×10^6	27.4×10^6
Activity (Ci/pin)	68,000	72,800
Decay heat (w/pin)	240	231
Neutrons per g Pu (n/s)	1,415	796
Neutrons per g TRU (n/s)	4.65×10^5	2.23×10^5
Specific heat (w/g Pu)	0.088	0.045
Specific heat (w/g TRU)	1.14	1.19

fission rate of the Pu isotopes varies from 0.424 at BOL to 0.677 at EOL, whereas for MOX fuel, it varies from 0.606 at BOL to 0.725 at EOL.

The reduced inventory of Pu per core loading and the greatly increased discharge burnup are likely to make Pu recycling with hydride fuel more economical. Economic analysis was beyond the scope of this work. The discharged PUZH fuel contains only 47.5% of the amount of Pu initially loaded into it versus 71.3% in the MOX fuel; both fuels operating for the same amount of time and generating the same amount of energy. The discharged mass of most actinides is larger for MOX than for PUZH fuel. The proliferation resistance of the downloaded PUZH Pu and MA is substantially higher because (1) the fissile Pu fraction is smaller; (2) the neutron emission per gram of Pu is 47% higher, and per gram of HM is 133% higher; and (3) the decay heat per gram of Pu is 38% higher and per gram of HM is 131% higher.

Handling of the discharged PUZH fuel requires similar precautions as of the MOX fuel: the decay heat and neutron emissions from the spent fuel assemblies are only 2.9 and 3.4% higher in PUZH as compared to MOX; the total activity and the gamma heating are 26 and 6.1% smaller in PUZH as compared to MOX.

All these characteristics contribute to making the PUZH fuel more effective for Pu incineration as well as more proliferation resistant than the MOX fuel.

6.4. Alternate hydride fuels

Preliminary analysis was performed on the transmutation capability of two alternate hydride fuels – the inert-matrix fuel PuH_2–$ZrH_{1.6}$, and a thorium containing hydride fuel PuH_2–ThH_2 (Ganda and Greenspan, 2005a, b, this issue). It was found that soluble boron is sufficient for excess reactivity adjustment of the Th-containing hydride-fueled core but cannot be used as the only means to compensate for the excess reactivity in case of the PuH_2–$ZrH_{1.6}$ fuel. The use of burnable poisons is necessary in this latter case to obtain a negative CTC of reactivity. But the use of burnable poison reduces the attainable discharge burnup and, therefore, the attainable fractional transmutation of the PuH_2–$ZrH_{1.6}$-fueled core. A better transmutation effectiveness is offered by the Th-containing hydride-fueled core. Selected performance characteristics of this core are compared in Table 13 against those of the reference MOX core.

It is found that using thorium for the fertile fuel it is possible to incinerate 62.5% of the loaded Pu in one pass through the core of a PWR that is uniformly loaded with hydride fuel. All the reactivity coefficients remain negative throughout the core life.

6.5. Conclusions

For Pu loading that gives the reference PWR cycle length when using the reference PWR core geometry, PUZH achieves more than double the average discharge burnup than MOX fuel, when both fuels are uniformly distributed throughout the core. All the reactivity coefficients are found negative along the entire fuel cycle. The least negative is the CTC of PUZH at the beginning of cycle because of its relatively high concentration of soluble boron. The use of a small mount of IFBA reduces the critical soluble boron concentration sufficiently to obtain negative reactivity coefficients.

Relative to MOX fuel, the recycling of Pu in PUZH fuel in the reference PWR geometry offers doubling of the fraction of Pu transmuted, smaller fissile Pu fraction in the discharged fuel, reduction of the inventory of MA generated, a higher decay heat and neutron emission rate per unit mass of Pu or TRU, smaller inventory of ^{237}Np and its precursors (Ganda and Greenspan, this issue), but comparable radiation levels and decay heat per discharged fuel assembly. As a result, the use of PUZH rather than MOX fuel is expected to significantly increase the effective repository capacity. The higher specific neutron yield and decay heat in the discharged TRU is expected to make the spent PUZH fuel more proliferation resistant than the MOX fuel, while the handling of the spent fuel assemblies are expected to require similar precautions as for the MOX fuel.

Using thorium hydride instead of zirconium hydride and eliminating the uranium, it is possible to obtain an even better fractional transmutation – incinerating 62.5% of the loaded Pu. Even higher fractional transmutation may be attained by design optimization.

The scoping study performed over a wide design space found (Ganda and Greenspan, this issue) that the peak burnup of PUZH fuel is achieved in a tighter lattice (P/D = 1.5–1.6) than for MOX fuel (P/D = 1.7–1.9). This could enable PUZH cores to operate at a higher power density than possible with MOX cores. This feature, along with smaller Pu inventory, is likely to make PUZH-fueled PWRs more economical than MOX-fueled PWRs.

It is recommended to thoroughly investigate the feasibility of recycling Pu in PWRs as well as in BWRs using hydride fuel of different compositions.

7. BWR – design approaches and methodology

7.1. Introduction

The objective of the work reported in this section is to assess the feasibility of improving the economics of BWRs by using hydride fuel instead of oxide fuel. BWRs are expected to benefit more than PWRs from hydride fuel implementation since, in order to achieve approximately the same hydrogen to HM ratio as that of PWRs, when fueled with oxide they need a coolant to fuel volume ratio about 1.5 times higher than PWRs. Hence, to compensate for the low hydrogen density of the boiling water, oxide-fueled BWRs have extra-moderation zones, as shown in Fig. 28, consisting of water rods and wide water gaps between the fuel bundles. The latter also provide space for the insertion of cruciform control rods and instrumentation tubes. From the moderation viewpoint, hydride fuel does not need these special moderation zones, whose volume could be used for insertion of additional fuel rods, yielding a core power density increase. However, while the elimination of water rods only is a minor design change yielding the so-called Backfit core configuration, the simultaneous elimination (or size reduction) of the water gaps – yielding the so-called NewCore configuration, is more challenging since it requires redesigning the core and reactor internals – particularly control rods, instrumentation tubes and structure of fuel bundles and their orificing systems.

Please cite this article in press as: Greenspan, E., et al., Hydride fuel for LWRs—Project overview. Nucl. Eng. Des. (2009), doi:10.1016/j.nucengdes.2008.11.023

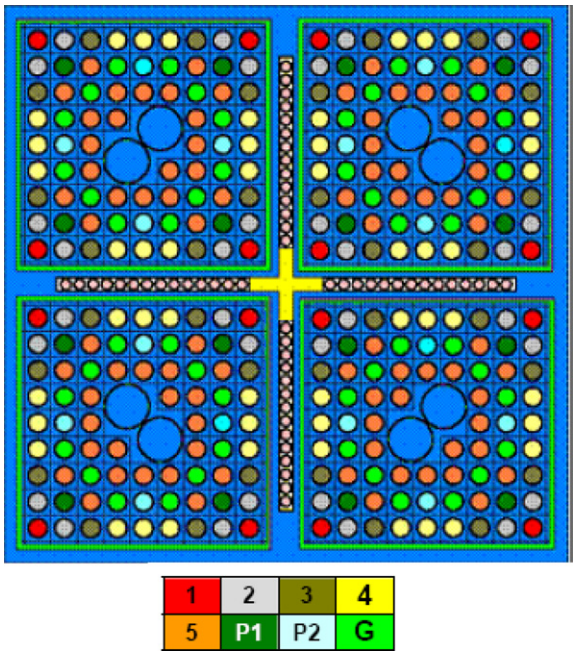

Fig. 28. Cross-sectional view of four 9 × 9 oxide-fueled bundles used as reference BWR bundle design. Color code: 1–5, full-length fuel rods of five different enrichment levels; P1 and P2, partial-length fuel rods; G – fuel rods containing gadolinia.

Water rod elimination and water gap width reduction allow designing hydride fuel bundles with (1) fewer enrichment levels than required for oxide fuel, resulting in less heterogeneous lattice, and (2) a flatter pin-by-pin power distribution, with a maximum local pin peaking factor ranging between ~1.04 for the most optimistic scenario and ~1.11 for the most pessimistic scenario. A typical pin-wise peaking factor for oxide fuel is around 1.11.

7.2. Study scope

The scope of the BWR analysis was limited; neutronic and thermal hydraulic analyses were not consistently coupled, fuel rod vibration analysis was not performed in detail, while transient and fuel rod mechanical integrity analysis were not performed. Moreover, core hydrodynamic stability performance was not explicitly calculated; rather, the susceptibility of the cores analyzed to instability phenomena was qualitatively limited by constraining the core average exit quality (in the whole-core analysis) and the hot bundle average exit quality (in the single-bundle analysis) to the values of the reference BWR. This does not guarantee avoidance of instability phenomena; however, it prevents operation at high-quality conditions, where BWRs are more susceptible to hydrodynamic instabilities. The neutronic and thermal hydraulic analyses were coupled indirectly as follows: (1) Core axial and radial power distributions were assumed to be the same for oxide and hydride cores and equal to those of a typical oxide-fueled BWR. It appears reasonable that hydride-fueled BWRs can be designed to have similar power distribution as of oxide cores. (2) The in-bundle pin power distribution was calculated using accurate 3D neutronic analysis. (3) The void fraction axial distribution of a typical oxide-fueled BWR was used for the neutronic analysis of both oxide and hydride cores. Again, this appears a reasonable assumption because the hydride-fueled core can be designed to have a similar axial void distribution. These assumptions enabled comparison of the power density and other characteristics expected from the hydride-fueled BWR relative to those of the oxide-fueled BWR based on the comparison of single fuel bundles of identical outer dimensions. Nevertheless, the conclusions of the BWR study are only indications of possible performance gains; more detailed consistent analysis needs to be done before firm conclusions can be drawn.

Table 14
Selected reference BWR design and performance parameters.

Parameter	Value
Geometry	
Vessel inner radius (m)	3.188
Core shroud radius (m)	2.605
Total number of bundles	764
Bundle heated length (m)	3.708
Bundle total length (m)	4.180
Bundle lattice	9 × 9
Fuel rod outer diameter (mm)	11.18
Fuel rod pitch (mm)	14.38
Full-length fuel rods per bundle	66
Partial length fuel rods per bundle	8
Equivalent full-length fuel rods per bundle	~71
Water rods per bundle	2
Bundle orificing	2 zones: central (648 bundles), periphery (116 bundles)
Operating conditions	
Core pressure (MPa)	7.136
Core inlet temperature (°C)	278.3
Core thermal power (MW)	3323
Coolant flow rate through the core (kg/s)	13671
Maximum assembly radial peaking factor	1.51
Maximum axial peaking factor	1.47
Maximum local peaking factor	1.28

The BWR work consisted of neutronic, thermal hydraulic, and economic analyses. The objective of the neutronic analysis was to identify the acceptable combinations of fuel rod outer diameter, D, and the square lattice pitch to diameter ratio, P/D – referred to as "geometry", of hydride as well as oxide fuels and to quantify the attainable discharge burnup. To be acceptable a geometry must have negative fuel and CTCs of reactivity as well as negative void reactivity feedback throughout the core life. The objective of the thermal hydraulic analysis was to estimate the maximum power density attainable using different geometries, both oxide- and hydride-fueled, subjected to a number of design constraints. The objective of the economic analysis was to use the results from the neutronic and thermal hydraulic analyses to estimate the COE attainable from BWRs designed with hydride fuel versus oxide-fueled BWRs.

The neutronic, thermal hydraulic, and economic analyses, which are discussed in detail in the specific papers (Fratoni et al. (this issue); Ferroni et al. (this issue); Ganda et al. (this issue-b)), are summarized in, respectively, Section 7.4, Section 7.5, and Section 7.6. Section 7.3 provides a brief description of the BWR core chosen as reference.

7.3. Reference reactor

The BWR/5 and the 9 × 9 fuel bundle of Fig. 28 are used as the reference reactor and reference bundle, respectively. Table 14 summarizes key parameters of the reference reactor (Ferroni et al., this issue). The fact that the power density of the oxide fuel bundle and core selected as reference is low relative to more advanced BWR designs (loaded with 10 × 10 bundles) does not affect the comparison between hydride and oxide fuels performed in this work, as we are searching for maximum power density oxide and hydride bundle designs using the same set of assumptions, constraints, and methodology.

7.4. Neutronics

The approach adopted for this study is to first estimate an upper bound to the possible power density gain relative to the reference oxide fuel bundle design shown in Fig. 28. This is done by exam-

Please cite this article in press as: Greenspan, E., et al., Hydride fuel for LWRs—Project overview. Nucl. Eng. Des. (2009), doi:10.1016/j.nucengdes.2008.11.023

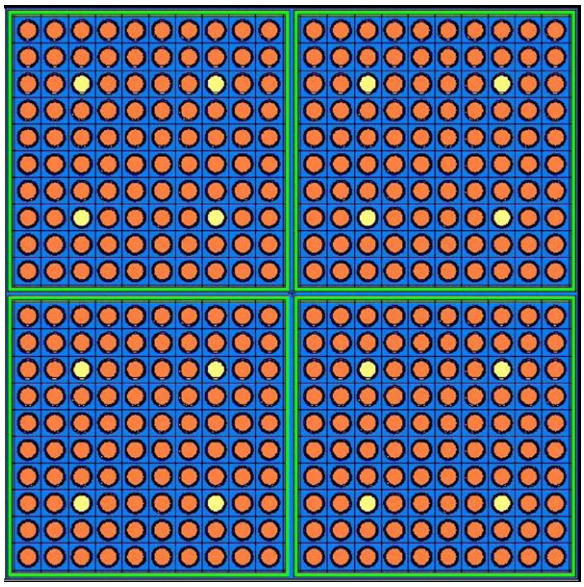

Fig. 29. Layout of four Idealized hydride fuel bundles, 10×10 array per bundle containing 96 fuel rods with uniform enrichment and four control rods.

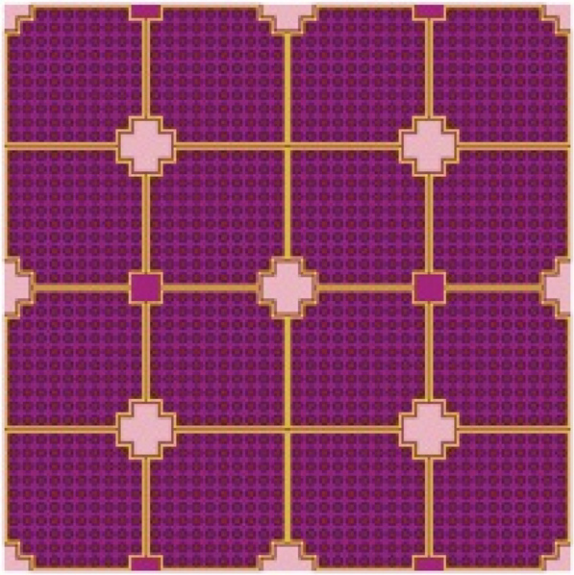

Fig. 30. Layout of 16 hydride fuel bundles design with cruciform corner control rods (CCCR) and corner space for instrumentation.

ining the "Idealized" bundle design shown in Fig. 29. It features the minimum feasible space in-between the fuel bundles and the most uniform hydride fuel bundle concept possible.[11] The reactivity control is provided in this idealized design using control rods inside the bundle. Then two practical hydride fuel bundle designs are studied; the corner cruciform control rods (CCCR) design and the control blade (CB) design. They were conceived to minimize the space occupied by the water gaps while providing space for instrumentation tubes and avoiding the design challenge of control elements insertion inside the bundle. The CCCR design features truncated cruciform-shaped control rods at the bundle corners outside the bundle box (Fig. 30), while the CB design uses more

[11] This bundle concept is referred to as "Idealized" because (a) it appears very difficult, if not impractical, to design the control rods to penetrate into the bundle and (b) it does not provide space for instrumentation tubes.

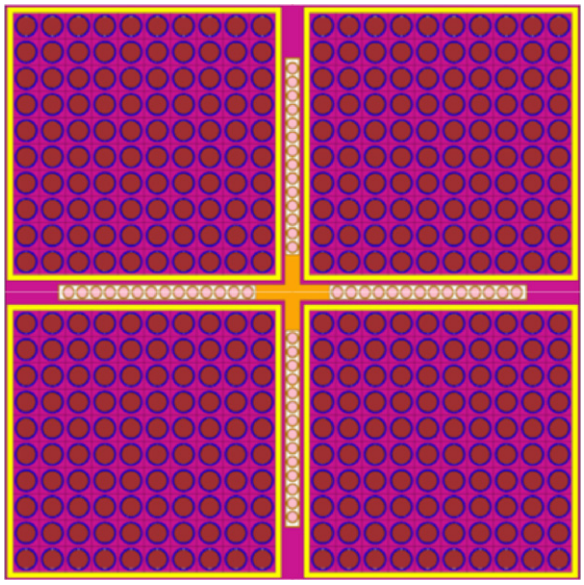

Fig. 31. Layout of four hydride fuel bundle design with control blades (CB) and narrow water channels.

conventional cruciform CBs in-between the fuel bundles; however, the water gap between bundles is minimized on two sides of the bundle (Fig. 31). Both the CCCR and the CB designs are intended for newly built BWRs.

The bundle pitch of all hydride bundles considered is the same as of the reference oxide bundle shown in Fig. 28. Relative to the 71 effective full-length fuel rods of the reference 9×9 oxide fuel bundle, the hydride fuel bundles examined have, in the order presented, 96, 93, and 100 full-length fuel rods. The first two hydride fuel bundles have a similar, while the third bundle has a slightly smaller fuel rod diameter than of the reference oxide fuel bundle. The performance of these hydride fuel bundles was also compared against that of a 10×10 oxide fuel bundle that has thinner fuel rods.

The neutronic feasibility study consists of three parts, all involving a 3D fuel bundle analysis. The first part is a scoping analysis that covers a limited number of fuel rod outer diameters, D, for a given pitch, P. The objective of this scoping analysis is to identify the geometry, i.e., D–P combination that offers the maximum achievable burnup. The second part of the study is a detailed neutronic analysis of this maximum burnup fuel bundle as well as of a bundle offering a larger power level identified in the companion study (Ferroni et al., this issue). All the above studies examined the "Idealized" hydride fuel bundle concept. The last part of the study examines the two alternative (CCCR and CB) hydride fuel bundle designs that are more practical to implement.

The 3D neutronic analysis was performed using the MOCUP code system accounting for a typical axial water density distribution. Twenty-four depletion zones were considered for the reference oxide bundle, corresponding to eight groups of fuel rods and three average axial enrichments per group. Being of significantly more uniform design, only nine depletion zones were considered for hydride fuel bundles – three equal length axial and three radial zones. A four-batch fuel management scheme was assumed for estimating the discharge burnup, core average, k, and reactivity coefficients.

The statistical uncertainty in calculating k was $<5 \times 10^{-4}$ such that, after propagation through the k averaging procedure, the uncertainty in the core average k was $<2 \times 10^{-3}$.

Please cite this article in press as: Greenspan, E., et al., Hydride fuel for LWRs—Project overview. Nucl. Eng. Des. (2009), doi:10.1016/j.nucengdes.2008.11.023

Table 15
Bundle designs examined in the single-bundle analysis.

	Oxide 9 × 9 (ref.)	Oxide 10 × 10	Hydride 9 × 9	Hydride CCCR	Hydride CB	Hydride 10 × 10 idealized
Core configuration	Backfit	Backfit	Backfit	Alternative NewCore	Alternative NewCore	Idealized NewCore
D (mm)	11.18	10.26	11.18	11.18	10.71	10.80
P/*D*	1.286	1.262	1.286	1.300	1.300	1.300
Pellet-clad gap filler	He	He	LM	LM	LM	LM
FLFRs	66	78	81	93	100	96
PLFRs	8	14	0	0	0	0
Water rods	2	2	0	0	0	0
Control fingers	0	0	0	0	0	4
Active flow area, bottom and top (cm^2)	97.2 and 105.0	92.5 and 104.1	100.0	104.9	104.9	117.0
Wetted perimeter, bottom and top (mm)	3282 and 3001	3636 and 3185	3371	3816	3914	4003
Hydraulic diameter, bottom and top (mm)	11.84 and 14.00	10.18 and 13.07	11.87	11.00	10.72	11.69
Bundle unit width (mm)	152.4	152.4	152.4	152.4	152.4	152.4
Inter-bundle gap width (mm)	12.24	12.19	12.24	2	12.19 (blade side), 2 (blade-free side)	2
Active flow rate (as % of total flow rate)	86	86	90	95	94	96
Maximum pin peaking factor	1.28	1.28, 1.05(BC)	1.05(BC), 1.11(WC)	1.04 (BC), 1.11 (WC)	1.04 (BC), 1.11 (WC)	1.05

BC – best case; WC – worst case.

7.5. Thermal hydraulics

The thermal hydraulic study consisted of two independent analyses: a whole core analysis, performed for both oxide and hydride fuel over 400 geometries, i.e., 400 *D*–*P*/*D* combinations, and a single bundle analysis, performed in greater detail on a limited set of oxide and hydride fuel bundles. Matlab and the VIPRE-EPRI code were coupled to perform the whole-core analysis while the single-bundle analysis needed use of the VIPRE code only.

The whole-core analysis was mainly a scoping study, since the large range of bundle geometries examined required that simplifying assumptions be made. Among them, the assumption of the same bundle-wise pin power peaking factor, regardless of the fuel type and bundle geometry, is the most conservative. While the power density results derived from this analysis are consequently approximated, this analysis gave important insight about the range of bundle geometries that promise maximum power.

In the single-bundle analysis, in which the bundle modeling was performed with greater detail of geometric and rod power distribution than that characterizing the whole core analysis, the performance of two oxide fuel bundles were compared to those of four hydride fuel bundles three of which were introduced in Section 7.4. Table 15 summarizes key geometric characteristics of the six bundles examined. The oxide bundles were the reference 9 × 9 bundle of Fig. 28, representing the GE11 design, and a 10 × 10 bundle resembling the GE14 design. Both are for a Backfit core configuration. The hydride bundles examined were:

For Backfit core configuration:

- 9 × 9 bundle: it represents the least challenging way to retrofit the reference core since *D* and *P* are the same as in the reference GE11 bundle

For NewCore configuration:

- Idealized 10 × 10 design: shown in Fig. 29, this hydride bundle design was chosen to provide an upper bound of the power gain attainable with hydride fuel. The corresponding core configuration is consistently called “Idealized NewCore”.
- CCCR design (hydride CCCR) and CB design (hydride CB): these two designs, shown in Figs. 30 and 31, are for a core configuration that, because of the water gap reduction and modified out-of-bundle control rods, is called the “Alternative NewCore”.

In the single-bundle analysis,[12] all the bundle designs examined have the same cross-sectional area (including the surrounding water gap), the same operating pressure and coolant inlet temperature (Table 14), the same axial power distribution, the same form loss coefficients, and the same subchannel-averaged exit quality.[13] The pellet-clad gap was assumed to be filled with helium in oxide bundles and with LM (Pb–Bi–Sn eutectic) in hydride bundles. The low fuel temperature limit for hydride fuel, i.e., 750 °C, along with a need for protecting the Zircaloy clad from hydrogen motivates the use of LM bonding (Olander et al., this issue). In terms of maximum attainable power density, however, the use of a LM for hydride bundles does not constitute an inherent advantage, since the use of the same gap filling material in oxide bundles does not cause their maximum achievable power to increase; the fuel temperature was never the power-limiting constraint for He-bonded oxide-fueled bundles.

The constraints applied in the single-bundle analysis are defined in Table 16. Two pressure drop limits were applied: a conservative value of 0.147 MPa is the pressure drop of the reference design and a 50% higher value of 0.220 MPa. The higher-pressure drop limit was chosen to account for an optimistic scenario in which not only a higher-pressure drop can be accommodated but also the higher coolant flow rate yielding that pressure drop. The results referred to this scenario need, however, to be verified since no bundle hold-down device design was developed to accommodate the increase in bundle lift-off forces resulting from the higher flow rates, and no calculation of the structural stability against vibrations of the steam dryers was performed.

[12] Details about the whole-core analysis, not discussed here, can be found in Ferroni et al. (this issue).

[13] The value chosen for the subchannel-average exit quality, i.e. 25.1%, derives from the reverse engineering analysis of the hot bundle of the reference oxide core. Therefore, even though the analysis of each bundle was not preceded by a whole-core flow distribution analysis, the fact that less coolant flows through the hot bundle relative to the average bundle is accounted for by assuming that, for all the hydride cores regardless of the power level, the ratio between the hot bundle flow rate and the average bundle flow rate is the same, and it is equal to that of the reference oxide BWR.

Please cite this article in press as: Greenspan, E., et al., Hydride fuel for LWRs—Project overview. Nucl. Eng. Des. (2009), doi:10.1016/j.nucengdes.2008.11.023

Table 16
Constraints used in the steady-state single-bundle analysis.

	UO_2	$U–ZrH_{1.6}$
MCHFR	≥1.213	≥1.213
Fuel centerline temperature, (°C)	<2805	<750
Fuel average temperature, (°C)	<1400	N.A.[a]
Clad surface temperature, (°C)	<349	<349
Bundle pressure drop (MPa)	≤0.147 ≤0.220	≤0.147 ≤0.220
Subchannel averaged exit quality (%)	25.1	25.1

[a] Not applied.

Table 17
Neutronic performance characteristics of oxide and hydride fuel bundles.

Parameter	Oxide 9 × 9	Hydride 10 × 10	
		P/D = 1.15	P/D = 1.30
Number of fuel rods	~71	96	96
Number of control rods	Control blades	4	4
P/D	P.I.[a]	1.15	1.30
Pellet diameter (cm)	0.955[b]	1.061	0.936
Fuel rod outer diameter (cm)	1.118[b]	1.264	1.118
Average enrichment (%)	3.90	5	5
Initial HM mass ratio	1.00	0.68	0.53
Single batch BOL k_∞	1.404	1.370	1.381
Burnup (GWd/tHM)	43.5	52.0	48.0
Fuel residence time (EFPD)	1740	1412	1012

Not accounting for burnable poisons.
[a] Information proprietary to G.E.
[b] Watford (1997).

7.6. Economics

The economic analysis methodology adopted is based on the levelized lifetime COE (AEN-NEA, 2005; OECD/NEA, 1994; Saccheri et al., 2008) that evaluates the amount of money that should be charged per unit of generated electricity to recover exactly the production cost. The latter is conventionally divided into three components: (1) capital costs, (2) operation and maintenance costs, and (3) fuel cycle costs. Bracketing values are used for the overnight construction costs ($1970 and $3010/kW), for the power-scaling factor (0.4 and 0.8), and for the discount rate (5 and 10%). Additional assumptions and details about the methodology are given by Ganda et al. (this issue-b).

8. BWR – results

8.1. Neutronics

A detailed 3D neutronic analysis was performed for the oxide and hydride fuel bundles to determine attainable discharge burnup, pin-by-pin power distribution, reactivity coefficients, reactivity worth of control elements, and burnable absorber effects. Table 17 compares selected characteristics of the maximum burnup (P/D = 1.15) and close to maximum power[14] (P/D = 1.30) idealized hydride-fuel bundle (Fig. 29) versus the reference oxide core design. Even though the hydride fuel bundle has 96 full-length fuel rods versus only 71 effective full-length oxide fuel rods in identical core volume, the HM inventory in the hydride fuel bundles is smaller. So although the hydride fuel burnup is higher, its cycle length is shorter than that of the reference oxide fuel bundle. A longer cycle can be obtained by increasing the initial enrichment; it is estimated that with enrichment of ~7.7% for P/D = 1.15 or ~8.6% for P/D = 1.30, the hydride fuel cycle will be as long as that of the reference oxide fuel that has an average enrichment of 3.9%, when operated at the same power per bundle.

All temperature and void coefficients considered are negative. The reactivity worth of the control rods of the idealized hydride fuel bundles is found comparable to (in case of P/D = 1.15) or larger (P/D = 1.30) than the worth of the cruciform shaped control elements in the reference oxide fuel bundle. The larger control rods worth of the hydride fuel P/D = 1.30 design is due to a softer neutron spectrum of this design relative to the P/D = 1.15 design and to the smaller HM inventory. The cold shutdown margin is short, for all three designs examined in Table 17, of the ~5% required. This is probably due to the neglect of burnable poisons in this analysis and, possibly, also to ignoring of the leakage effect from the finite core. If necessary, the shutdown margin can be increased by loading the control rods with boron enriched in ^{10}B instead of natural boron.

A limited study was undertaken to evaluate possible choices of burnable poisons for the hydride-fueled BWRs. This analysis focused on the maximum burnup idealized hydride bundle design (P/D = 1.15) and compared it to the reference oxide-fueled BWR. Gadolinia is used as burnable poison in the oxide fuel bundle; it is added in 12 rods at two different weight fractions – 4.5% at the top and 5.5% at the bottom of the core. The use of gadolinia reduces the attainable burnup from 43.5 to 37.5 GWd/tHM and increases the variation in the BOC pin-wise power distribution from 1.11 to 1.21. Of four types of burnable poisons examined for hydride fuel, IFBA was found the preferred one since it minimizes the burnup penalty to 6 GWd/tHM while maintaining the flattest pin-wise power distribution; the peak-to-average pin power is 1.05. All the hydride fuel designs with burnable poisons offer negative reactivity coefficients over the entire cycle length and are, therefore, neutronically feasible. Table 18 compares selected characteristics of BWR designed with either one of the two more practical hydride fuel bundles with those of the idealized hydride fuel bundle. Without use of graded enrichment levels the pin-wise power distribution in the CCCR and CB designs are not as flat as in the idealized design.

8.2. Thermal hydraulics

Tables 19 and 20 compare the bundle performance characteristics when none of the constraints of Table 16 is exceeded and the pressure drop limit is fixed at the lower and upper limit respectively, i.e., at 0.147 and at 0.220 MPa. The key parameters for the comparison are the maximum achievable bundle power, Q_{bundle}, and the power difference percentage with respect to the reference bundle, ΔQ_{bundle}. Table 20 shows the power difference percentage with respect to the oxide 10 × 10 bundle, $\Delta Q_{bundle10}$, as well. The tables also show the active flow rate m_{act} and the value of each characteristic for which a constraint is applied: minimum critical heat flux ratio (MCHFR), maximum fuel centerline temperature ($T_{f,max}$), maximum fuel average temperature ($T_{f,avg}$), maximum clad surface temperature ($T_{c,out}$), bundle pressure drop (Δp), and subchannel averaged exit quality (x_{out}). Highlighted numbers represent characteristics matching the corresponding limit. The following acronyms are used in the tables: BC (best case), WC (worst case), CCCR (corner cruciform control rod) design, and CB (control blade) design.

It can be seen from Table 19 that, except for the "idealized" 10 × 10 hydride design, when the pressure drop limit is fixed at the lower value, i.e., 0.147 MPa, the hydride bundles deliver approximately the same power as the reference oxide bundle. However, when the pressure drop is constrained to the upper limit, i.e., 0.220 MPa, an appreciable power gain is possible (Table 20): it is about 26% for the Backfit hydride 9 × 9 bundle and about 32% for the alternative NewCore hydride designs (CCCR and CB). These power gain percentages decrease to 16 and 22% when the comparison is

[14] Based on the results of the whole-core analysis performed in the companion thermal hydraulic study (Ferroni et al., this issue), it is expected that the maximum power attainable by an idealized hydride bundle is not significantly higher than that attainable by the P/D = 1.3 geometry.

Please cite this article in press as: Greenspan, E., et al., Hydride fuel for LWRs—Project overview. Nucl. Eng. Des. (2009), doi:10.1016/j.nucengdes.2008.11.023

Table 18
Neutronic and other characteristics of alternative designs of hydride fuel bundles.

Parameter	Idealized	CCCR	CB
Fuel rod OD (m)	1.118	1.118	1.071
P/D	1.30	1.30	1.30
Number of fuel rods	96	93	100
Bundles gap thickness (cm)	0.2	0.2	0.2/1.22
Control system	4 control rods inside bundle	2 corner cruciform control rods	Control blades
Neutron absorber	Natural B	90%-enriched B	Natural B
BOC core average k_∞ at zero power cold shutdown conditions compared to the reference oxide core (%)	−0.56	+0.00	−0.22
HM loading (kg/bundle)	91	88	87
Burnup (GWd/tHM)	48.0	46.0	47.7
Fuel residence time (EFPD)	1012	940	960

Table 19
Maximum power achievable by selected bundles with Δp_{limit} = 0.147 MPa (constraints reached are highlighted, single-bundle analysis).

Parameter	Oxide 9 × 9 (ref)	Oxide 10 × 10	Hydride 9 × 9 (BC)	Hydride 9 × 9 (WC)	Hydride CCCR (BC)	Hydride CCCR (WC)	Hydride CB (BC)	Hydride CB (WC)	Hydride 10 × 10 idealized
m_{act} (kg/s)	15.54	14.74	15.39	15.34	15.94	15.93	15.84	15.85	17.96
MCHFR	1.213	1.296	1.358	1.375	1.434	1.370	1.395	1.392	1.358
$T_{f,max}$ (°C)	1978	1605	500	511	477	489	462	474	497
$T_{f,avg}$ (°C)	1247	1046	N.A.[a]	N.A.	N.A.	N.A.	N.A.	N.A.	N.A.
$T_{c,out}$ (°C)	311	310	306	306	305	305	304	305	306
Δp (MPa)	0.147	0.147	0.147	0.147	0.147	0.147	0.147	0.147	0.147
x_{out} (%)	25.1	25.1	25.1	25.1	25.1	25.1	25.1	25.1	25.1
Q_{bundle} (kWh)	6568	6246	6540	6517	6786	6776	6733	6730	7623
ΔQ_{bundle} (%)	0	−4.9	−0.4	−0.8	+3.3	+3.2	+2.5	+2.5	+16.1

[a] Not Applied as a constraint per Table 16.

Table 20
Maximum power achievable by selected bundles with Δp_{limit} = 0.220 MPa (constraints reached are highlighted, single-bundle analysis).

Parameter	Oxide 9 × 9 (ref)	Oxide 10 × 10	Hydride 9 × 9 (BC)	Hydride 9 × 9 (WC)	Hydride CCCR (BC)	Hydride CCCR (WC)	Hydride CB (BC)	Hydride CB (WC)	Hydride 10 × 10 idealized
m_{act} (kg/s)	15.54	16.76	19.49	19.48	20.30	20.32	20.14	20.13	22.67
MCHFR	1.213	1.213	1.214	1.227	1.309	1.229	1.257	1.252	1.213
$T_{f,max}$ (°C)	1978	1852	555	570	527	543	509	523	551
$T_{f,avg}$ (°C)	1247	1182	N.A.[a]	N.A.	N.A.	N.A.	N.A.	N.A.	N.A.
$T_{c,out}$ (°C)	311	312	310	310	309	309	308	308	310
Δp (MPa)	0.147	0.183	0.220	0.220	0.220	0.220	0.220	0.220	0.220
x_{out} (%)	25.1	25.1	25.1	25.1	25.1	25.1	25.1	25.1	25.1
Q_{bundle} (kWh)	6568	7108	8285	8282	8642	8647	8555	8551	9628
ΔQ_{bundle} (%)	0.0	+8.2	+26.1	+26.1	+31.6	+31.6	+30.2	+30.2	+46.6
$\Delta Q_{bundle10}$ (%)	−7.6	0.0	+16.6	+16.5	+21.6	+21.6	+20.4	+20.3	+35.4

[a] Not Applied as a constraint per Table 16.

made with respect to the oxide 10 × 10 bundle. Table 21 shows the power gains that could be expected in case it was possible to ignore the pressure drop constraint. Up to 40% gain is expected relative to the power of the 10 × 10 oxide fuel. The required pressure drop is 0.284 MPa; nearly, 100% higher than the nominal (0.147 MPa). Such a pressure drop may be impractical because the corresponding total core flow rate will probably harm the steam dryer structural stability and cause excessive lift-off forces on the bundles.

Table 21
Maximum power achievable by selected bundles with no limit on the pressure drop[a]. (Constraints reached are highlighted, single-bundle analysis).

Parameter	Oxide 9 × 9 (ref)	Oxide 10 × 10	Oxide 10 × 10 (BC)	Hydride 9 × 9 (BC)	Hydride 9 × 9 (WC)	Hydride CCCR (BC)	Hydride CCCR (WC)	Hydride CB (BC)	Hydride CB (WC)	Hydride 10 × 10 idealized
m_{act} (kg/s)	15.54	16.76	17.13	19.51	19.82	23.41	20.95	21.82	21.35	22.67
MCHFR	**1.213**	**1.213**	**1.213**	**1.213**	**1.213**	**1.213**	**1.213**	**1.213**	**1.213**	**1.213**
$T_{f,max}$ (°C)	1978	1852	1873	555	575	563	551	527	537	551
$T_{f,avg}$ (°C)	1247	1182	1200	N.A.[b]	N.A.	N.A.	N.A.	N.A.	N.A.	N.A.
$T_{c,out}$ (°C)	311	312	309	310	310	311	309	309	309	310
Δp (MPa)	0.147	0.183	0.188	*0.221*	*0.227*	*0.284*	*0.234*	*0.254*	*0.244*	0.220
x_{out} (%)	**25.1**	**25.1**	**25.1**	**25.1**	**25.1**	**25.1**	**25.1**	**25.1**	**25.1**	**25.1**
Q_{bundle} (kWh)	6568	7108	7256	8294	8427	9968	8917	9272	9068	9628
ΔQ_{bundle} (%)	0.0	+8.2	+10.5	+26.3	+28.3	+51.8	+35.8	+41.2	+38.1	+46.6
$\Delta Q_{bundle10}$ (%)	−7.6	0.0	+2.1	+16.7	+18.6	+40.2	+25.4	+30.4	+27.6	+35.4

[a] Numbers in italics indicate pressure drops higher than the upper pressure drop limit used in this analysis (0.220 MPa).
[b] Not Applied as a constraint as per Table 16.

Please cite this article in press as: Greenspan, E., et al., Hydride fuel for LWRs—Project overview. Nucl. Eng. Des. (2009), doi:10.1016/j.nucengdes.2008.11.023

Table 22
Summary of the reduction in the COE offered by hydride-fueled BWR using 10%-enriched uranium relative to the COE of the reference oxide-fueled BWR that uses an average enrichment of 3.94%.

Fuel type	CCCR	CCCR	CB	CB	CCCR (BC)
Core pressure drop constraint (MPa)	0.147	0.220	0.147	0.220	None[a]
$1970/kW – 0.4 scaling factor[b] (%)	−2.6	−14.7	−2.5	−14.5	−20.8
$1970/kW – 0.8 scaling factor (%)	−1.9	−9.3	−2.0	−9.3	−13.0
$2490/kW – 0.4 scaling factor (%)	−2.9	−15.0	−2.8	−14.8	−21.1
$2490/kW – 0.8 scaling factor (%)	−2.2	−9.1	−2.3	−9.1	−12.6
$3010/kW – 0.4 scaling factor (%)	−3.2	−15.3	−3.1	−15.1	−21.5
$3010/kW – 0.8 scaling factor (%)	−2.4	−9.0	−2.4	−8.9	−12.3

[a] Power is MCHFR limited.
[b] The "scaling factor" is "x" in the assumed capital cost, C, escalation with power level, P; $C = C_{ref}\,(P/P_{ref})^x$ (Ganda et al., this issue-b).

8.3. Economics

Table 22 summarizes the results of the economic analysis. Given in the table is the reduction in the COE generated in a BWR that is designed with one of the three hydride fuel bundles relative to the COE of the reference oxide-fueled BWR that uses an average uranium enrichment of 3.94%. Using 5% instead of 3.94% average enrichment for the reference 10×10 oxide fuel bundles the COE advantage of hydride fuel is estimated to be lower by the values reported in Table 22 by about 1.7 and 8–10% for, respectively, a core pressure drop of 0.147 and 0.220 MPa. Part of this difference might be compensated by increasing the hydride fuel enrichment to ~12.5% that was found in the PWR economic analysis (Shuffler et al., this issue-b) to provide a lower COE than 10%-enriched uranium.

It is concluded that the COE from a newly constructed BWR reactor loaded with hydride fuel bundles can be significantly lower than the COE from the typical BWR loaded with oxide fuel bundles. The cost saving depends on the core pressure drop constraint that can be implemented in newly constructed BWR. It is between 2 and 3%, between 9 and 15%, or between 12 and 21% when the core pressure drop constraint assumed is, respectively, that of the reference BWR, 50% higher or close to 100% higher. The attainable cost reduction was found insensitive to the specific construction cost but strongly depends on the power-scaling factor. The cost advantage of hydride-fueled cores as compared to that of the oxide reference cores depends only weakly on the uranium and SWU prices, on the "per volume base" fabrication cost of hydride fuels, and on the discount rate used.

8.4. Discussion

It was found possible to design hydride fuel bundles for BWRs that are significantly less heterogeneous than present day oxide fuel bundles and that can operate at a higher power density without violating any of the steady-state design constraints used in this study, provided that (1) the core pressure drop could be increased above that of the reference BWR design value and (2) stability performance of hydride cores, not investigated in this study, is acceptable. Two factors contribute to the power density increase: (a) a larger total clad surface area per core volume, obtained by increasing the number of fuel rods and (b) flatter pin-wise power distribution.

The higher power density of hydride fuel cores could be used either to increase the total power attainable from a given core volume or a given reactor vessel volume, or to reduce the length (or volume) of the core. The former approach may be of interest for a new generation of the ABWR, whereas the latter approach may become of interest to the ESBWR.

The hydride fuel bundles have reduced HM inventory per bundle. Consequently, to obtain comparable cycle length, the hydride fuel needs to have higher uranium enrichment than oxide fuel. A potentially promising approach for obtaining long cycles is to use thorium-containing hydride fuels; the HM content of thorium-based hydride fuel is more than double that of the U–$ZrH_{1.6}$ fuel considered in this work; it is even larger than that of oxide fuel. Use of Pu for the primary fissile fuel is another promising approach.

A number of important feasibility issues need to be assessed and the study needs to be refined and extended before final conclusions can be drawn on the possible benefits from using hydride fuel in BWR cores. Future undertakings should include: (1) detailed mechanical design of the hydride fuel bundle and of the control elements and their drive mechanism; the minimum practical water gap between bundle boxes needs to be determined; (2) design of pumps, core structure, and vessel internal components for higher coolant pressure drop; (3) determination of burnable poison and enrichment distribution in hydride fuel bundles; (4) coupled neutronic – thermal hydraulic analysis; (5) hydrodynamic stability analysis; (6) full scope transient and accident analysis; (7) study of compatibility of hydride fuel with BWR water and clad.

9. Summary and conclusions

The feasibility study reported in this overview paper and detailed in the set of 11 accompanying topical papers has established that hydride fuel can safely operate in PWRs and BWRs without restricting the core power density of these reactors relative to that attainable with oxide fuel. However, the study only addressed design performance feasibility issues but could not fully consider important material compatibility issues, including the compatibility of hydride fuel with PWR and BWR coolants and clad. These material compatibility issues need to be experimentally addressed before a sound conclusion can be drawn on the desirability of developing hydride fuel for commercial LWRs.

The study identified a number of promising applications of hydride fuel in both BWRs and PWRs:

(1) Eliminating dedicated water moderator volumes in BWR cores, thus enabling a significant increase in the fuel rod surface area as well as in the coolant active flow cross-section area in a given fuel bundle volume while significantly reducing the fuel bundle heterogeneity, thus achieving flatter pin-by-pin power distribution. The net result depends on the core pressure drop that can be accommodated. If the pressure drop is not allowed to increase above the reference core value, an optimistic power density increase relative to the reference 9×9 oxide-fueled BWR is only about 15%, with more likely values below 10%. If the pumping system is upgraded so that a pressure drop 50% higher than the reference core value can be accommodated, the most optimistic power density increase is estimated to be around 45%, with more likely values around 30%. These power density gains decrease by about 10% if the comparison is made with respect to cores loaded with a more recent commercial design of high-performance 10×10 oxide fuel bundles. Even though hydride fuel requires 10–12.5%-enriched uranium, the power density gain offered by hydride fuel results in a sig-

Please cite this article in press as: Greenspan, E., et al., Hydride fuel for LWRs—Project overview. Nucl. Eng. Des. (2009), doi:10.1016/j.nucengdes.2008.11.023

nificant reduction in the COE from newly constructed BWRs compared to presently used as well as newly constructed oxide-fueled BWRs. Achievement of high-power density gains require significant core and internals design modifications that could probably be achieved only in newly designed plants. A hydride bundle design optimization, not performed in this study, can further increase the power density attainable from hydride fuel. However, detailed stability and safety analysis may limit the power density and, hence, the economic benefit from hydride fuel.

(2) Recycling Pu in PWRs more effectively than is possible with oxide fuel by virtue of several unique features of hydride fuel-reduced inventory of ^{238}U, increased inventory of hydrogen, and fixation of a significant fraction of the hydrogen in the fuel. As a result of these features, the amount of Pu that needs to be loaded into the hydride core to provide the reference cycle length is only 84% that needed for MOX cores, and the hydride core neutron spectrum is softer. Due to these characteristics, the hydride-fueled core achieves more than double the average discharge burnup – about 115 GWD/MTHM versus 55 GWD/MTHM of MOX. The total Pu inventory in the discharged PUZH fuel is only 47.5% of the initially loaded inventory versus 71.3% in the discharged MOX fuel. The net amount of Pu consumed per cycle is 55% larger with PUZH versus MOX fuel. The corresponding fissile Pu to total Pu ratio is 45% versus 60%. The corresponding ratio of MA to Pu concentration at discharge is 10.5% versus 7.0%. The total neutron source strength at discharge of PUZH fuel is 825 n/s/g of Pu and 2.3×10^4 n/s/g of HM versus 561 and 9.9×10^3 n/s, respectively for MOX fuel. The decay heat levels are 21.1×10^{-3} w/g HM for PUZH and 9.1×10^{-3} w/g HM for MOX fuel. Nevertheless, the decay heat and neutron emissions from the spent fuel assemblies are only 2.9 and 3.4% higher in PUZH as compared to MOX; the total activity and the gamma heating are 26 and 6.1% smaller in PUZH as compared to MOX, because of the difference in HM inventory and composition.

Even though not studied in this project, we expect that use of hydride fuel will also significantly improve the capability of BWRs to recycle Pu.

Likewise, even though not considered in this project, we expect that hydride fuel will also significantly improve the minor actinide recycling capability of both PWRs and BWRs.

Additional findings of this work include the following:

(1) The optimal oxide-fueled PWR core design features a smaller fuel rod diameter of 6.5 mm and a larger P/D ratio of 1.39 than presently practiced by industry – typically 9.5 mm and 1.326. This optimal design can provide a 27% increase in the power density and a 19% reduction in the COE provided the PWR could be designed to have the coolant pressure drop across the core increased from the reference 0.20 MPa to 0.414 MPa.

(2) Using wire-wrapped oxide or hydride fuel rods in hexagonal fuel assemblies, it is possible to design PWR cores to operate at 54% higher power density than the reference PWR design that uses grid spacers and a square lattice, provided a 0.414 MPa coolant pressure drop across the core could be accommodated. Uprating existing PWRs to use such cores could result in a 40% reduction in the COE. The optimal oxide lattice geometry is $D = 9.34$ mm and $P/D = 1.37$.

(3) Three approaches that can turn the positive CTC of reactivity of U–$ZrH_{1.6}$-fueled PWR cores to be negative were identified for the D–P design range offering peak power:
   a. Use of erbium burnable poison.
   b. Replacement of some of the $ZrH_{1.6}$ by ThH_2.
   c. Use of Pu rather than enriched uranium as the primary fissile material.

   Of the three, use of erbium is the least desirable since it penalizes the attainable discharge burnup, even if the erbium is enriched in the isotope ^{167}Er. Replacement of some of the Zr hydride by Th hydride can, actually, somewhat increase the attainable discharge burnup. The use of Pu is also effective but is practical only when Pu recycling is desirable.

(4) The BOL prompt reactivity feedback due to fuel temperature increase is more negative when using U–$ZrH_{1.6}$ fuel than when using UO_2 fuel due to a unique feature of hydride fuel – spectrum hardening due to fuel hydrogen temperature increase. This prompt spectrum-hardening effect is superimposed on and enhances the Doppler effect. However, the EOL prompt reactivity feedback is not as negative as is the BOL feedback because of the buildup of ^{239}Pu that turns the fuel hydrogen-induced spectrum hardening to have a positive contribution to the prompt fuel temperature reactivity feedback.

(5) The transmutation capability of inert-matrix hydride fuel PuH_2–$ZrH_{1.6}$ is constrained by positive reactivity coefficients. However, using PuH_2–ThH_2 fuel (with some depleted uranium added for denaturing the ^{233}U), it is possible to transmute at least 62.5% of the loaded Pu in one recycle in PWR, using uniform composition fuel assemblies. Further optimization is required to identify maximum fractional transmutation using hydride fuel.

Possible new reactor design concepts and design innovations were arrived at during the project based on the results generated in this study and the insight provided by these results:

(1) IC design in which the hydride fuel is made of hexagonal fuel prisms, which are penetrated by cylindrical water coolant channels arranged in a hexagonal array. Hydride fuel makes such a geometry feasible by virtue of its fabrication process – it is first cast as a metal alloy in the desirable shape, and then turned into hydride by diffusion of hydrogen it is exposed to. The inverted geometry features reduced coolant friction losses for a given FCR relative to conventional core designs featuring cylindrical fuel rods held in place by grid spacers. This latter feature enables designing the IC to have a larger fuel volume fraction, a feature of particular benefit for hydride fuel. Our preliminary study suggests that the IC with twisted tape can achieve a higher power relative to the optimal hydride-fueled pin-geometry core. The power of one promising twisted tape design is estimated at 6870 MW, which is 135% of the optimally powered hydride pin-geometry design (5080 MW). This design, however, has fuel web and clad thickness just below our acceptable ranges. Upon design optimization, using reasonable values for fuel web and clad thickness, we expect the inverted design power to be only slightly reduced.

(2) Hexagonally shaped fuel assemblies with wire-wrap support as considered for many LM-cooled fast reactor designs. This array is similar to the Russian PWR (VVER) design approach except that wire wraps are used instead of grid spacers. This design approach features significantly lower pressure drop than the conventional grid-spacer design especially, in the high-fuel volume fraction design range – a range that was expected to be preferred for hydride fuel. It was found, however, that at the coolant pressure range considered in this study, hydride fuel was not advantageous compared to oxide fuel. Additional attributes of the wire-wrap design are higher critical heat flux and improved fuel rod vibrations characteristics.

(3) Axial power flattening of BWR cores by using hydride fuel made of deuterium at the lower part of the core, and made of regular hydrogen at the upper part of the core. This design approach is

Please cite this article in press as: Greenspan, E., et al., Hydride fuel for LWRs—Project overview. Nucl. Eng. Des. (2009), doi:10.1016/j.nucengdes.2008.11.023

expected to enable designing BWR cores to have more uniform axial distribution of hydrogen and, therefore, more uniform moderation and more symmetric axial power distribution. This design approach has not been analyzed, as yet.

(4) Reduction of the heavy water inventory and the capital cost required for heavy-water reactors by replacing the oxide fuel by hydride fuel. Alternatively, it may be possible to replace the D_2O moderator by graphite without having to increase the pitch between the pressure tubes, i.e., the reactor volume while providing sufficient distance between the pressure tubes to provide convenient access for the on-line refueling machines. In case that graphite is used for the moderator, no calandria tubes may be required, further simplifying the design. This reactor concept has not been studied, as yet.

(5) Incineration of trans-uranium actinides (TRUs) in PWRs that use $U–ZrH_{1.6}$ or, even better, $U–ZrH_{1.6}–ThH_2$ as "driver fuel" in part of the core, and $TRUH_2–ZrH_2$ as "incinerating fuel" in another part of the core. The driver fuel could use 20%-enriched uranium, while the incinerating fuel is a hydride version of an "inert-matrix" fuel. The TRU to be loaded in this incinerating fuel includes all the Pu and MA generated in the driver fuel. Alternatively, $PuH_2–U–ZrH_{1.6}–ThH_2$ could be used for the driver fuel for enhanced incineration of the Pu or of MA.

10. Recommendations

The feasibility studies reported upon in this special issue of *Nuclear Engineering and Design* concluded that the nuclear industry might substantially benefit from hydride fuel provided hydride fuel is compatible with LWRs. It is therefore highly recommended to first of all embark upon a thorough assessment of the compatibility of hydride fuel with (1) water and (2) zirconium-based clad material at PWR and BWR-operating conditions.

It is also recommended to assess the feasibility of fabricating hydride fuel made of U, $ZrH_{1.6}$, and ThH_2 as well as hydride fuel made of PuH_2 and $ZrH_{1.6}$ and investigate their compatibility with LWRs coolant conditions.

An additional recommended undertaking is a thorough safety analysis of hydride fuel-loaded PWR and BWR cores, as well as a stability analysis of hydride-fueled BWRs.

Feasibility assessment of the new design options identified in this study (at the end of previous sections) is also recommended.

Acknowledgments

This work was supported by US DOE NERI under award number DE-FG07-02SF22615 and monitored by Dr. Madeline Feltus.

Help provided by Dr. Russ M. Fawcett of GNF for the BWR study is highly appreciated.

References

AEN-NEA, 2005. Projected cost of generating electricity. 2005 Update, OECD.
Diller, P., Todreas, N., Hejzlar, P., this issue. Thermal hydraulic analysis for wire wrapped PWR cores.
Ferroni, P., Handwerk, C., Todreas, N., this issue. Steady-state thermal hydraulic analysis of hydride-fueled grid-supported BWRs.
Fratoni, M., Ginex, F., Ganda, F., Greenspan, E., this issue. Neutronic design of hydride fueled BWRs.
Ganda, F., Greenspan, E., 2005a. Incineration of Pu in PWR using hydride fuel. In: Proceedings of the International Conference on Advances in Nuclear Power Plants; ICAPP–2005, Seoul, Korea.
Ganda, F., Greenspan, E., 2005b. Plutonium incineration capability of hydride versus MOX fuel in PWR. In: Proceedings of GLOBAL'05, Tsukuba, Japan, October 9–13, p. 2005.
Ganda, F., Greenspan, E., 2005c. A simplified method for multi-batch PWR core analysis based on SAS2H unit cell calculations. In: Proc. Int. Mtg. Mathematics and Computation–MC2005, Avignon, France.
Ganda, F., Barnes, D., Greenspan, E., 2005. OECD benchmark A & B of MOX fueled PWR unit cells using SAS2H. In: Proc. Int. Mtg. Mathematics and Computation–MC2005, Avignon, France.
Ganda, F., Greenspan, E., this issue. Plutonium recycling in hydride fueled PWR cores.
Ganda, F., Greenspan, E., Petrovic, B., this issue-a. Reactor physics analysis for PWR cores.
Ganda, F., Shuffler, C., Greenspan, E., this issue-b. Economic analysis for BWRs.
Garkisch, H.D., Petrovic, B., 2004. Proposed correlations for cladding thickness and fuel-cladding gap for UO_2 and U-ZrH fuel in PWRs. Westinghouse Electric Company LLC. NERI02-189-WEC-04.
Greenspan, E., Todreas, N., Petrovic, B., 2002. Use of solid hydride for improved long-life LWR core designs, NERI Project Number 02-189.
Greenspan, E., Garkisch, H., Malen, J., Moalem, M., Olander, D., Petrovic, B., Shayer, Z., Todreas, N., 2003. Preliminary assessment of possibilities for improving the performance of LWRs using hydride fuel. Trans. Am. Nucl. Soc. 89, 381–382.
Greenspan, E., Ganda, F., Garkisch, H., Malen, J., Petrovic, B., Romano, A., Shayer, Z., Shuffler, C., Todreas, N., Trant, J., 2005. Optimization of UO_2 fueled PWR core design. In: Proceedings of the International Conference on Advances in Nuclear Power Plants; ICAPP–2005, Seoul, Korea.
Iorgulis, C., Ciocanescu, M., Preda, M., Mladin, M., 1998. Neutronic calculations regarding the new LEU 6×6 fuel bundle for 14 MW TRIGA-SSR, in order to increase the reactor power up to 21 MW. Int. Mtg. on Reduced Enrichment for Research and Test Reactors, Sao Paulo, Brazil.
Malen, J.A., Todreas, N.E., Romano, A., 2004a. EquationThermal hydraulic design of hydride fueled PWR cores. In: Proceedings of the 6th International Conf. on Nuclear Thermal Hydraulics, NUTHOS-6, Nara, Japan.
Malen, J.A., Todreas, N.E., Romano, A., 2004b. Thermal hydraulic design of hydride fueled PWR cores. MIT Department of Nuclear Science and Engineering, Report MIT-NFC-TR-062.
Malen, J., Todreas, N., Hejzlar, P., Ferroni, P., Bergles, R., this issue. Thermal Hydraulic design of a hydride-fueled PWR cores.
OECD/NEA, 1994. The Economics of the nuclear fuel cycle. OECD Publications, Paris.
Olander, D., Garkisch, H., Petrovic, B., Greenspan, E., this issue. Hydride fuel materials performance and design constraints.
Romano, A., Shuffler, C., Garkisch, H., Olander, D., Todreas, N., this issue. Fuel performance analysis for PWR cores.
Saccheri, J.G.B., Todreas, N.E., Driscoll, M.J., June 2008. Design and economic evaluation of an advanced tight-lattice core for the small-scale IRIS integral pressurized water reactor. Nuclear Technology 158, 2008.
Shuffler, C., Trant, J., Todreas, N.E., Romano, A., 2006. Thermal hydraulic and economic analysis of grid-supported, hydride- and oxide-fueled PWRs. MIT Department of Nuclear Science and Engineering, Report MIT-NFC-TR-077.
Shuffler, C., Malen, J., Trant, J., Todreas, N., this issue-a. Thermal hydraulic analysis for grid supported pressurized water reactor cores.
Shuffler, C., Malen, J., Diller, P., Ganda, F., Todreas, N. Greenspan E. and Petrovic, B., this issue-b. Economic analysis for PWRs.
Shwageraus, E., Hejzlar, P., Kazimi, M.S., 2003. Feasibility of multirecycling of Pu and MA in PWRs using combined non-fertile and UO_2 (CONFU) fuel. In: Proc. GLOBAL'03, New Orleans, LA.
Simnad, M.T., 1981. The U-ZrHx alloy: its properties and use in TRIGA fuel. Nucl. Eng. Design, 64, 403–422. Also General Atomic Report GA-A16029, 1980.
Simnad, M.T., 1986. An Assessment of thorium hydride or deuteride as a reactor fuel matrix. Reprint from the archives of Prof. Mike Driscoll of MIT Nuclear Engineering Department.
Taiwo, T.A., Kim, T.K., Stillman, J.A., Hill, R.N., Salvatores, M., Finck, P.J., 2003. Assessment of a heterogeneous PWR assembly for plutonium and minor actinides recycle. In: Proc. GLOBAL'03, New Orleans, LA.
Trant, J. M., 2004. Transient analysis of hydride fueled pressurized water reactor cores, M.Sc. Dissertation, MIT Department of Nuclear Engineering.
Trellue, H.R., 2004. Neutronic and logistic proposal for transmutation of plutonium from spent nuclear fuel as mixed-oxide fuel in existing light-water reactors. Nucl. Tech.
Tsuchiya, B., Huang, J., Konashi, K., Saiki, W., Onoue, T., Yamawaki, M., 2000. Thermal diffusivity measurement of uranium-thorium-zirconium hydride. J. Alloys Compd. 312, 104–110.
Wright, R.F., Tulenko, J.S., Schoessow, G.J., Connell, R., Dubecky, M.A., Adams, T., 1996. Nuclear Technol. 115, 281–292.
Yamamoto, T., Suwarno, H., Ono, F., Kayano, H., Yamawaki, M., 1998. Preparation, analysis and irradiation of hydrided U–Th–Zr alloy samples for a new fuel. J. Alloys Compd. 271–273, 702–726.
Yamawaki, M., Suwarno, H., Yamamoto, T., Ono, F., Yamaguchi, K., Kayano, H., 1997. Development of MA-containing hydride fuel as MA burning target material. In: Proceedings of the International Conference on Future Nuclear Systems, GLOBAL'97, Yokohama, Japan.
Yamawaki, M., et al., 1999. Development of U–Th–Zr alloy hydrides as alternative thorium-base fuel and MA burning target fuel. In: Proceedings of the International Conference on Future Nuclear Systems, GLOBAL'99, Jackson Hole, WY.
Youinou, G., Zaetta, A., Vasile, A., Delpech, M., Rohart, M., Guillet, J.L., 2001. Heterogeneous assembly for plutonium multirecycling in PWRs: The CORAIL concept. In: Proc. Global'01, Paris, France.

Please cite this article in press as: Greenspan, E., et al., Hydride fuel for LWRs—Project overview. Nucl. Eng. Des. (2009), doi:10.1016/j.nucengdes.2008.11.023